A peer-reviewed version of this preprint was published in PeerJ on 4 February 2016.

Khang TF, Soo OYM, Tan WB, Lim LHS. 2016. Monogenean anchor morphometry: systematic value, phylogenetic signal, and evolution. PeerJ 4:e1668 https://doi.org/10.7717/peerj.1668

Running head: ANCHOR MORPHOMETRY FOR MONOGENEAN SYSTEMATICS

Title: Monogenean Anchor Morphometry: Systematic Value, Phylogenetic Signal, and Evolution

Authors: Tsung Fei Khang[1*], Oi Yoon Michelle Soo[2], Wooi Boon Tan[3], Lee Hong Susan Lim[2+]

[1]*Institute of Mathematical Sciences, Faculty of Science, University of Malaya, 50603 Kuala Lumpur, Malaysia.*

[2]*Institute of Biological Sciences, Faculty of Science, University of Malaya, 50603 Kuala Lumpur, Malaysia.*

[3]*Centre for Tropical Biodiversity Research, University of Malaya, 50603 Kuala Lumpur, Malaysia.*

*Corresponding author

+Deceased on 2 August 2014

Email: tfkhang@um.edu.my

Tel: +603 79674171

Fax: +603 79674143

ABSTRACT

Anchors are important attachment appendages that prevent the physical dislodging of a monogenean parasite from fish host gills. Common descent and evolutionary processes have left their mark on anchor morphometry, in the form of patterns of shape and size variation useful for systematic and evolutionary studies. We used a geometric morphometric approach to explore anchor shape variation in 13 *Ligophorus* (Monogenea:Ancyrocephalidae) species infecting two marine mugilid (Teleostei: Mugilidae) fish hosts (*Moolgarda buchanani* and *Liza subviridis*) in the waters off West Peninsular Malaysia. Molecular sequence data from three nuclear markers: 28S rRNA, 18S rRNA and ITS1, were used to infer a maximum likelihood phylogeny to enable visualization of shape evolution in phylomorphospace. For inferring patterns of size evolution in the phylogeny, we used a size measure based on the first principal component of all pairwise Euclidean distances between landmarks. Cluster heat map and principal component analysis showed that anchor shape variation had sufficient systematic information for delimiting 12 of the 13 species. Adams' multivariate K test indicated significant correlation between anchor shape and phylogeny (p-value = 0.0001). We also discovered that characters based on anchor shaft shape, the length between inner and outer root tips and the length between inner root tip and the dent point were more phylogenetically informative than inner and outer lengths, as indicated by a maximum parsimony tree that was better resolved and had major clades congruent with those of the molecular phylogenetic tree. Continuous character mapping of size onto the inferred molecular phylogeny and Rayleigh's test for departure from directional uniformity in each species's landmark relative to the ancestor indicated that species infecting *M. buchanani* generally evolved larger and more robust anchors, while those infecting *L. subviridis* generally evolved smaller and more delicate anchors. Nevertheless, phylogenetic regression of anchor shape against body size and anchor size showed significant correlation (p-value =

0.02) between anchor shape and size, suggesting morphometric constraints in anchor evolution. Finally, morphological integration analysis revealed tight integration between the root and point compartments within anchors, confirming that the anchor functions as a single, fully integrated module. The present work is supported by the development of integrative analytical tools in the form of a new R package – `monogeneaGM`. By lowering barriers to data integration and analysis, we aim to encourage the scientific community to collect and contribute morphometric and genetic data from other *Ligophorus* species, which are essential for developing *Ligophorus* as a model system for understanding association between patterns of anchor shape size evolution and biodiversity in the Monogenea.

Keywords: cluster heat map - geometric morphometrics - *Ligophorus* - molecular phylogeny - Monogenea – morphological integration – phylogenetic regression - phylomorphospace - principal component analysis - size and shape variation

INTRODUCTION

The Monogenea is a class of flatworms (Platyhelminthes) that are primarily ectoparasites of fish (Whittington, 2005; Hayward, 2005). An adult monogenean parasite has well-developed attachment appendages located at its anterior (prohaptor) and posterior (opistohaptor) regions that help it to resist physical dislodgement from the host. The posterior attachment organs consist of sclerotized hard parts such as hooks, anchors and clamps. Ecologically, monogenean parasites are characterized by their strong host specificity (Whittington et al., 2000). The Monogenea has several desirable features that make it invaluable as a model system for studying evolutionary processes that resulted in its past diversification and present diversity (Poulin, 2002). Primarily, many of its genera are

speciose, morphologically diverse, show well-resolved phylogenies, and samples can be easily obtained in large numbers. It has been used as a model to shed light on ecological forces that shape species community and structure (Rohde, 1979), to investigate processes leading to speciation and its maintenance (Rohde and Hobbs, 1986; Rohde 1994; de Meeus et al., 1998; Šimková et al., 2002), to elucidate host-parasite evolutionary ecology (Huyse et al., 2003; Huyse and Volckaert, 2005; Mouillot et al., 2005; Šimková et al., 2006; Šimková and Morand, 2008), and to explore the extent of correlation between phenotype variation in attachment organs and factors such as phylogeny, host specificity and geographical location (Vignon et al., 2011).

Morphometric variation in anatomical structures of interest can be studied using two approaches. Traditional morphometrics (Reyment et al., 1984; Marcus, 1990) is characterized by the use of lengths of defined positions on anatomical structures of interest (or their ratios) as input data for multivariate statistical analyses. While such variables may measure size adequately, they are generally not effective for capturing shape information present in the geometry of a set of defined points of an object (Rohlf and Marcus, 1993). A large proportion of biological variation due to shape differences is therefore missed when an analysis uses only information from variation in length variables.

With the development of geometric morphometrics over the past three decades, researchers now have, at their disposal, a powerful method for extracting, visualizing and combining shape data with other data types such as molecular phylogenies to attain an integrative evolutionary analysis (Rohlf and Marcus, 1993; Adams et al., 2004; Adams et al., 2013). Digitization of the anatomical structure of interest provides the key to the acquisition and use of a new type of data - landmark coordinates, from which shape information can be effectively extracted, and then analyzed, using new tools such as Procrustes superimposition, thin plate splines, relative warp analysis and elliptic Fourier analysis. Geometric

morphometrics is now commonly used in systematics and evolutionary biology research where analysis of shape can be expected to provide new insights to complement traditional morphometric, phylogenetic or biogeographic analyses. A cursory search in major biological journal databases for recent publications having "geometric morphometrics" in their keywords revealed that geometric morphometrics is widely used to study various biological aspects, in diverse phyla, such as fish taxonomy (Sidlauskas et al., 2011), plant taxonomy (Conesa et al., 2012), gastropod shell shape variation (Smith and Hendricks, 2013; Cruz et al., 2012), morphological adaptation in birds (Sievwright and Macleod, 2012), fly wing evolution (Pepinelli et al., 2013), turtle neck shape evolution (Werneburg et al., 2015), beetle speciation (Pizzo et al., 2013) and species boundary problems in butterflies (Barão et al., 2014). Because of the inherently digital nature of geometric morphometric data, its increasing prominence in morphological studies accentuates the role of informatics in modern taxonomy (Wheeler, 2007).

In morphological analyses of monogeneans, taxonomists often prioritize prominent sclerotized parts such as copulatory organs, because qualitative variation in the latter is frequently sharp and easy to describe. Nonetheless, morphometric variation in all sclerotized parts of monogeneans has been studied for a long time from the perspective of systematics (e.g. Shinn et al., 2001) and evolutionary ecology (e.g. Poisot and Desdevises, 2010; Mendlová and Šimková, 2014). Hard parts such as anchors are ideal for geometric morphometric analysis because they are not easily deformed by compression when mounted onto slides (Lim and Gibson, 2009). The analysis of monogenean morphometric data has been, and continues to be, dominated by the application of traditional morphometrics (e.g. Mariniello et al., 2004; Shinn et al., 2004; Tan et al., 2010; Hahn et al., 2011; Soo and Lim, 2012). As a result, although anchors are the primary opistohaptor attachment organ, systematic information in the morphometry of anchors is seldom fully exploited in taxonomic

studies of monogeneans. To date, there are only few examples (Vignon and Sasal, 2010; Vignon, 2011; Vignon et al., 2011; Rodríguez-González et al., 2015) of applying geometric morphometrics to analyze monogenean anchor shape variation to overcome the limitations of traditional morphometric analyses. The paucity of geometric morphometric studies, however, belies the importance of this approach in uncovering intraspecific shape variation in anchors, that can be invaluable for species delimitation, particularly in resolving synonymys (e.g. Pérez Ben et al., 2014), as well as for testing hypotheses of morphological integration (Olson and Miller, 1958) and evaluating levels of phenotypic plasticity (Pfennig et al., 2010).

As anchors serve a functional purpose, a priori, it is unclear whether phenotypic similarity of anchors among species is an outcome of adaptive processes related to the ecology of their fish host, or simply a reflection of their phylogenetic constraint (Morand et al., 2002). If the presence of phylogenetic signal in anchors can be statistically established, evolutionary analysis of shape and size change can then be used to elucidate trends in particular clades. The results are expected to be useful for guiding the selection of appropriate anchor morphometric variables for conversion into morphological characters that have lower levels of homoplasy, thus overcoming the problem of unnecessary homoplasy of a morphological character arising from poor quality and insufficient number of character states (Perkins et al., 2009).

In this paper, we developed an integrative analysis that uses data from anchor morphometry and morphology, as well as DNA sequences that allows the investigation of broad aspects in the systematic biology of monogeneans, such as species delimitation, evolutionary ecology, phylogenetic signal, and morphological integration. For illustration, we used data obtained from 13 recently described species belonging to the *Ligophorus* (Monogenea: Ancyrocephalidae) genus, a particularly speciose genus with 62 species known to date (Soo et al., 2015).

151 MATERIAL AND METHODS

152 *Samples*

153 We collected 537 specimens (Table S1 in Supplementary Material) belonging to 13
154 *Ligophorus* species (Soo and Lim, 2012; Soo and Lim, 2015; Soo et al., 2015) from two
155 species of adult fish host: *Liza subviridis* Valenciennes, 1836 (n=52) and *Moolgarda*
156 *buchanani* Bleeker, 1853 (n=29) from several locations in tropical Western Peninsular
157 Malaysia (Fig. S1 in Supplementary Material). From 2009 to 2014, *Liza subviridis* was
158 collected off Carey Island in Selangor (2º 52' N, 101º 22' E), and *M. buchanani* off
159 Langkawi Island in Kedah (6° 21' N, 99° 48' E) and the sea off Johor (1° 20′N, 103° 32′ E).
160 Seven of the 13 species: *L. bantingensis* Soo & Lim, 2012, *L. careyensis* Soo & Lim, 2012,
161 *L. chelatus* Soo & Lim, 2012, *L. funnelus* Soo & Lim, 2012, *L. navjotsodhii* Soo & Lim,
162 2012, *L. parvicopulatrix* Soo & Lim, 2012 and *L. belanaki* Soo & Lim, 2015 were found on
163 *L. subviridis*; the remainder: *L. fenestrum* Soo & Lim, 2012, *L. kedahensis* Soo & Lim, 2012,
164 *L. kederai* Soo & Lim, 2015, *L. grandis* Soo, Tan & Lim, 2015, *L. johorensis* Soo, Tan &
165 Lim, 2015, and *L. liewi* Soo, Tan & Lim, 2015, were found on *M. buchanani*. For all 81 fish
166 examined, the *Ligophorus* species found in *M. buchanani* were never observed in *Liza*
167 *subviridis*, and vice versa. Thus, except for *L. bantingensis*, which was reported to be found
168 in *Liza abu* and *Liza klunzingeri* (Kritsky et al., 2013), the other species were considered as
169 specialists in the classical sense (Sasal et al. 1999).

170 When preparing slides, we used a basic mounting protocol (Lim, 1991) where the
171 monogeneans were put onto a clean slide with a drop of water, and then covered with a
172 coverslip. Specimens were initially mounted in modified ammonium picrate glycerine, and
173 subsequently converted into unstained, permanent mounts in Canada balsam. The
174 opistohaptorial sclerotized hard parts of *Ligophorus* consist of a pair (left and right) of dorsal
175 and ventral anchors, bars, and marginal hooks. Digital images of these hard parts were taken

from labelled mounted slides using a light microscope with Leica digital camera (DFC 320) connected to the QWin plus image analysis software (Leica Microsystems, Germany) under 40x magnification, saved as jpeg files and organized into folders. Three species (*L. fenestrum*, *L. liewi* and *L. kederai*) showed a probable fixed character state – that of the presence of fenestrated structures on anchors of all examined specimens, since no variation in this character state was observed in all examined specimens from these three species.

Data Acquisition

Where possible, we measured a specimen's body length from its anterior to posterior end, and body width at the midpoint of its body. To obtain landmark coordinate data from the anchors, we used TPSDIG2 (Rohlf, 2013; Rohlf, 2015). Eleven landmarks (LM) were placed sequentially on the right and left ventral and dorsal anchors of each specimen (Fig. 1). The set of all 11 landmark coordinates makes up a specimen's landmark configuration. Six of the landmarks are Type I (LM1,LM2,LM3,LM5,LM7,LM8), while the remainder (LM4,LM6,LM9,LM10,LM11) are Type III (i.e. semi-landmarks). LM1and LM3 are the inner and outer root points, respectively. Sandwiched between them is LM2, the groove point. LM5 is the dent point, while LM7 is the curve point. The tip point is represented by LM8. The semi-landmarks were defined relative to Type I landmarks. The horizontal (towards the outer root point) and vertical projections (towards the curve point) from LM2 intersect with the anchor outline to give LM4 and LM6, respectively. LM9 and LM10 are the intersection points between the vertical projection from LM7 and LM1 with anchor outline, respectively. The projection from LM2 perpendicular to the vertical projection from LM1 touches the anchor outline to define LM11. We used the set of landmarks LM1 to LM4 and LM11 to represent the shape of the root compartment, and the set LM5 to LM10 to represent the point compartment. For geometric morphometric analysis, semi-landmarks were not

specially treated (e.g. employing sliding landmark analysis), following Macleod (2013) that such treatments may introduce distortions to the original geometrical relationship that lead to complicated interpretations of the result.

Data Processing and Analysis Tools

We created a new R (Version 3.0.3; R Core Team, 2014) package called `monogeneaGM` (Khang, 2015) to process raw landmark coordinate data and integrate new methodological developments in the current study with numerous data processing and analysis tools in R packages such as `geomorph` (Adams and Otarola-Castillo, 2014), `phytools` (Revell, 2012), `circular` (Agostinelli and Lund, 2013), `gplots` (Warnes et al., 2014), `ape` (Paradis et al. 2004), `rgl` (Adler et al., 2014) and `cluster` (Maechler et al., 2013).

Data Quality Control

Despite careful slide preparation, it is inevitable that anchor images of some specimens would contain substantial amount of non-biological shape variation caused by incongruent image and object planes (Arnqvist and Mårtensson, 1998). The inclusion of these poor quality data in downstream analyses is undesirable, as they introduce noise into analysis that can potentially complicate the interpretation of results. To mitigate this problem, we developed a quality control procedure to filter out poor quality images. In this procedure, we first computed all pairwise Euclidean distances between landmarks for the left and right forms of dorsal and ventral anchors. If both left and right forms have congruent image and object planes, then by symmetry, their residual – the difference of their pairwise Euclidean distances for each landmark (M), should be close to zero, thus yielding a small sum of squared residuals (M^2). Moreover, we expect M to be randomly distributed with zero mean

across all average pairwise Euclidean distances (A) between the left and right forms. The slope of the regression equation of M against A (b) allows us to measure how well this expectation is satisfied. To be comparable with the sum of squared residuals, we squared the estimated regression slope (b^2), and then scaled it to be on the same order of magnitude as M^2. Thus, a good quality specimen would have small sum of M^2 and b^2, and vice versa. We defined the quality score Q, as

$$Q = 100 \times 10^{\frac{-\sqrt{M^2+b^2}}{10}}.$$

The magnitude of this measure is straightforward to interpret – it is high (maximum 100) for good quality specimens and low (minimum 0) for poor ones. Figure 2 shows examples of poor and good quality specimens together with their Tukey Mean-Difference (TMD) plots, respectively. Specimens with Q of 10 or more (n=443; Table S1 and Fig. S2 in Supplementary Material) were used for subsequent analyses.

Converting Pairwise Euclidean Distances in Arbitrary Units to Physical Units

We used a subset (n=97) of the total specimens with quality score above 10 (n=443) and measured the physical distances from LM1 to LM3 and from LM1 to LM5 in these samples using QWin plus image analysis software (Leica Microsystems, Germany). We then regressed the physical distances against the computed pairwise Euclidean distances to determine the linear equation for converting arbitrary distance units into their physical units (in µm). Thus, all pairwise Euclidean distances computed from raw landmark coordinates could be converted to physical distances by multiplication with a factor of 0.2 followed by addition of 0.9 (Fig. S3 in Supplementary Material).

Geometric Morphometric Analysis

For each species, we performed Generalized Procrustes Analysis (GPA; Gower, 1975; Rohlf and Slice, 1990) to align the sample landmark configurations for both ventral and dorsal anchors, using the `gpagen` function in the `geomorph` package (Version 2.1.1; Adams and Otarola-Castillo, 2014). The resulting GPA coordinates of the left and right forms were then averaged. GPA removes the effects of translation, rotation and scaling so that the resulting landmark configurations have minimum sum of squared distances with respect to the mean landmark configuration (Adams et al., 2004). Nevertheless, even after GPA, comparison of anchor shape variation can still be potentially confounded by the presence of non-biological variation in the landmark configuration. Specifically, if many samples of a species have anchors lying in one particular position, it would not be clear whether variation between its members' mean GPA landmark configuration and those of other species constitutes genuine biological variation or mathematical artifact. Typical application of geometric morphometrics in non-microscopic objects (fly wings, skulls, etc.) does not usually suffer from this problem, since specimens from species to be compared can be manipulated into standardized positions before imaging.

To ensure that the landmark configurations of all 13 species were comparable, we determined the angular deviation of LM7 from the $x=0$ line, and rotated all landmark coordinates by this amount with the origin as pivot. This has the effect of creating standardized landmark configurations for specimens across all species since the x-coordinate of LM7 is always zero after adjustment. The GPA coordinate data thus obtained were then organized into a data matrix with rows representing specimens and columns representing the 44 GPA landmark coordinates.

Molecular Phylogenetic Analysis

We used DNA sequence data from three nuclear markers: 28S rRNA, 18S rRNA and ITS1 from the 13 *Ligophorus* species to infer their phylogenetic tree. In doing so, we assumed that the species phylogeny is well-approximated by the phylogeny of these genes, though gene trees cannot be expected to always reflect the species tree (Maddison, 1997). Partial 28S rRNA and ITS1 sequence data were obtained from Soo et al. (2015), whereas 18S rRNA sequence data were generated in the present study. Briefly, the *Ligophorus* specimens were removed from host gills, identified morphologically and then preserved in 75% ethanol. Genomic DNA was extracted from samples using DNAEasy extraction kit (QIAGEN, Hilden, Germany). About 5µl of the extracted DNA was used as template in the PCR reaction to amplify the partial 18S rRNA sequence using two primers: WormA (5'-GCGAATGGCTCATTAAATCAG-3') (Littlewood and Olson, 2001) and new930F (5'-CCTATTCCATTATTCCATGC-3') (modified from Littlewood and Olson, 2001). The PCR reaction (50µl) was carried out in a solution containing 1.5mM $MgCl_2$, PCR buffer (Fermentas), 200µM of each deoxyribonucleotide triphosphate, 1.0 µM of each PCR primer and 1U of Taq polymerase (Fermentas), in a thermocycler (Eppendorf Mastercycler) using the following conditions: initial denaturation at 95°C for 4 minutes, followed by 35 cycles of 95°C, 52°C and 72°C for one minute each, with final extension at 72°C for 10 minutes. An aliquot (10µl) from the amplicons were electrophoresed in 1.3% agarose gel, stained with ethidium bromide and viewed under an ultraviolet illuminator. The remaining 40µl of each amplicon was purified using a DNA purification kit (QIAGEN, Hilden, Germany) and subjected to automated DNA sequencing (ABI 3730 DNA Sequencer, First Base Laboratories, Kuala Lumpur) using the same primers used for PCR amplification. Approximately 750 bp of the 18S rRNA sequence were amplified and sequenced for the 13 *Ligophorus* species (Table 1).

For sequence analysis, we concatenated the three nuclear markers for each species, and then aligned them using MAFFT (Version 7) with default parameters (Katoh and Standley, 2013). MEGA (Version 6; Tamura et al., 2013) was used to select, using Bayesian Information Criterion, the optimal DNA substitution model. The latter was subsequently used to build the maximum likelihood (ML; Felsenstein, 1981; Felsenstein, 2003) phylogenetic tree (partial deletion at 40% cut-off; 500 bootstrap replicates). We annotated the tree with the morphology of anchors, bars and male copulatory organ to allow visual assessment of overall phylogenetic and phenotypic correlation.

Species Delimitation

Delimiting a monogenean species is a complex art that involves the comparison of qualitative features of numerous anatomical structures: the male copulatory organ, female reproductive organ, anchors, bars and marginal hooks. Among the sclerotized hard parts, multivariate morphometric analyses of shape and size variables of suitable anatomical structures provide a quantitative means for species delimitation, which is invaluable for complementing the results from qualitative morphological analyses.

To visualize species clustering in low dimension morphospace, we applied Principal Component Analysis (PCA) separately for the ventral and dorsal anchors using their GPA coordinate data. The trade-off between loss of information through dimensional reduction and gain of interpretation via visualization in PCA can, however, make it difficult to judge how well members of the same species cluster together in the PCA scatter plots, especially when there are overlaps between different species clusters. To overcome this problem, we complemented PCA results with the cluster heat map (Wilkinson and Friendly, 2008), a powerful method for organizing high-dimensional multivariate data that allows visual detection of patterns of variation. The cluster heat map first maps numerical information in

the cells of the input data matrix to corresponding color codes. Then, a hierarchical clustering algorithm is applied to cluster the samples by similarity, in such a way that within cluster variation is always smaller than between cluster variation. For the current analysis, we estimated similarity between each pair of sample using the Euclidean distance metric. The resulting distance matrix was then used as input for hierarchical clustering of samples using the generalized Ward algorithm (Batagelj, 1988).

To assess the impact of applying the quality control procedure, we compared cluster heat maps generated using all samples, and using only samples that passed data quality control. Heat map construction was done using the `heatmap.2` function in the `gplots` package (Version 2.13.0; Warnes et al., 2014). We found the simple heat map a good alternative to inspection of the PC loadings table when trying to interpret the first few PC axes biologically.

Testing for Presence of Phylogenetic Signal in Anchor Shape

Species with different shapes are localized in particular regions of the morphospace. When a phylogeny is superimposed onto this morphospace, a phylomorphospace is induced, and it becomes possible to evaluate whether common descent or convergent evolution is likely to have shaped phenotypic similarity (Klingenberg and Ekau, 1996; Sidlauskas, 2008; Revell, 2014). If anchor shape contains substantial phylogenetic signal, then we expect the phylogeny to have non-random branching patterns in phylomorphospace. Graphically, we may visualize the latter by superimposing the molecular phylogeny of *Ligophorus* on the PCA plots of the first three principal components for the ventral and dorsal anchors. Estimation of ancestral node positions in the phylomorphospace was done using the maximum likelihood method as implemented in the `fastAnc` function of the `phytools` package (Version 0.4-21; Revell, 2012).We formally tested the presence of phylogenetic

signal in anchor shape by applying Adams's multivariate K test (Adams, 2014a), implemented using the `physignal` function (10 000 iterations) in the `geomorph` package (Version 2.1.1; Adams and Otarola-Castillo, 2013). Under the null hypothesis of absence of phylogenetic signal, the lineages of a given phylogeny are assumed to evolve randomly in phylomorphospace according to Brownian motion, which corresponds to the parameter value K=1. When phylogenetic signal is greater than expected, K > 1, and vice versa.

Analysis of Anchor Shape and Size Evolution

In studying anchor shape and size evolution, we were primarily concerned with trends occurring in different clades of the phylogeny of the 13 *Ligophorus* species. To control for the effect of body size in subsequent phylogenetic regression analysis of anchor shape against anchor size, it was necessary to first test for collinearity of body size and anchor size (Mundry, 2014). Since body size was prone to distortion during fixation, we used the median of body size and body width of each species to reduce the impact of outliers. For analysis, the logarithm (base 10) of the product of median body length and width was used.

The GPA landmark coordinates of the ancestral anchor were estimated using the maximum likelihood method as implemented in `fastAnc` function from the `phytools` package (Version 0.4-21; Revell, 2012) . Anchor shape change associated with a clade is statistically supported if mean directional change deviates significantly from uniformity in a set of landmarks. We visualized directional deviation in the 11 landmarks of both ventral and dorsal anchors using circular plots (Agostinelli and Lund, 2013; implemented in the `circular` package, Version 0.4-7). We then performed Rayleigh's test (Batschelet, 1981) to test for evidence against directional uniformity in each landmark. The strength of statistical evidence against mean directional uniformity in each landmark was assessed using p-value. Wireframe-lollipop plots (Klingenberg, 2013) were used to graphically summarize the mean

change in direction and mean magnitude of landmark displacement from root ancestor landmark configuration.

For investigating trends in anchor size evolution, we first computed all possible pairwise Euclidean distances between the raw landmarks in each sample. Each dorsal and ventral anchor has 11 landmarks, thus generating 55 possible pairwise Euclidean distances which we used as size variables. When the loadings and variables of the first principal component (PC1) have the same sign, PC1 can be interpreted naturally as a measure of size (Jolliffe, 2002). Subsequently, we performed continuous character mapping (implemented using `contMap` function in the `phytools` package) of mean PC1 of the size variables of each species for ventral and dorsal anchors onto the phylogeny of 13 *Ligophorus* species to assess clade-specific patterns of anchor size evolution. The Adams-Collyer phylogenetic regression for shape response variable (Adams, 2014b; Collyer et al. 2014; implemented in the `geomorph` package, Version 2.1.1) was used to formally test evolutionary correlation between anchor shape and two covariates: the logarithm of body size and logarithm of anchor size. The interaction between the two covariates was incorporated into the phylogenetic regression model if covariate collinearity could be ruled out using the Ho-Ané phylogenetic regression (Ho and Ane, 2014; implemented in the `phylolm` package, Version 2.2) under a Brownian motion model for the phylogenetic covariance matrix. For both regression analyses, p-values were computed via a resampling procedure with 10 000 iterations.

Covariation of Anchor Shape and Size with Copulatory Organ Morphology

Rohde and Hobbes (1986) hypothesized that the reproductive barrier among congeneric species that share the same host can be maintained in monogenean parasites by their having different copulatory organ morphology when attachment organs are similar (thus

occupying similar microhabitats); conversely, when parasites have dissimilar attachment organs (thus occupying different microhabitats), the morphology of their copulatory organs would not show important differences, since the lack of proximity puts less evolutionary pressure on the parasites to evolve different morphology for their copulatory organs. Qualitative evidence with limited number of congeneric species (Lambert and Maillard, 1975; Roubal, 1981; Rohde et al., 1994) supported the hypothesis's feasibility. Quantitative evaluations using larger species assemblage that relied on traditional morphometric data are available, but the interpretation of their results in support of the hypothesis was obscured by either the problem of using inflated degrees of freedom in regression analysis (e.g. Šimková et al., 2002) or failure to control for the effect phylogeny (e.g. Jarkovský et al., 2004). With the development of new tools for geometric morphometric and phylogenetic comparative methods, we are in a position to retest the Rohde-Hobbs hypothesis. To this end, we compared the size of the male copulatory organ (mean tube length, data from Soo and Lim, 2012, 2015; Soo et al., 2015) and three of its selected morphological characters (Table 2: position of copulatory organ entrance at main lobe of accesory piece; accesory piece of male copulatory complex; shape of accesory piece of male copulatory complex) against anchor shape and size variation. Ancestral node positions were estimated as before using the `fastAnc` function in the `phytools` package.

Morphological Integration Analysis

The roots of the anchor are bases for muscle attachment. Biomechanically, force exerted through muscles and transmitted to the point compartment controls the anchor's grip strength on the gills. Because of this, we may expect the anchor to be a single, fully integrated module (Klingenberg, 2008) on a priori grounds. Anchor shape is strongly constrained by either phylogeny or convergent evolution. By ruling out the latter explanation

statistically, suitable morphological characters based on variation in anchor shape can be expected to be systematically useful.

To date, only few morphological integration analyses in monogeneans have been done. Using published morphological drawings, Vignon et al. (2011) investigated interspecific modularity of attachment organs (marginal hooks, anchors and bars) in 66 *Cichlidogyrus* (Monogenea: Ancyrocephalidae) species. More recently, Rodríguez-González et al. (2015) studied intraspecific morphological integration of the root and the point compartments of anchors in *Ligophorus cephali*, using the partial least squares method in the context of shape analysis (Rohlf and Corti, 2000). Here, we extended their morphological integration analysis to the interspecific level in *Ligophorus*. We applied the phylogeny-aware partial least squares method based on the evolutionary covariance matrix (Adams and Felice, 2014) to estimate the extent of morphological integration between the ventral and dorsal anchors, as well as that of the root compartment (L1 to L4 and L11) and point compartment (L5 to L10) within and between the ventral and dorsal anchors.

New Morphological Characters from Morphometric Variables

A continuous morphometric variable can be discretized and treated as a morphological character with two or more states for use in a cladistic analysis (Thiele, 1993; Rae, 1998; Wiens, 2001). In doing so, the taxonomist relies on experience and intuition to select promising morphometric variables out of a potentially large set of candidates. Unfortunately, an objective means to screen the latter is generally lacking. As a result, it is difficult to assess the level of homoplasy present in the taxonomist's candidate characters. Here, we show how comparison of patterns of shape change in different clades leads to the discovery of new morphometric variables for morphological phylogenetic analysis in

449 *Ligophorus*. A set of 12 morphological characters defined in Sarabeev and Desdevises (2014)
450 that are not invariant for the 13 *Ligophorus* species (Table 2; see Table S3 in Supplementary
451 Material for character state matrix) was chosen. We replaced the morphological characters
452 derived from traditional morphometric measurements of anchors with new candidates derived
453 from geometric morphometric analysis to assess their phylogenetic informativeness. To this
454 end, we compared how well-resolved the resulting maximum parsimony trees (using PAUP;
455 Swofford, 2002) were. Tree search (initial tree obtained via stepwise addition) was performed
456 using the heuristic search option. Branch-swapping was done using the tree bisection and
457 reconnection algorithm. Tree reliability was assessed using 1000 bootstrap replicates and
458 branches were collapsed if bootstrap support was below 50%.
459
460 RESULTS
461 *Molecular Phylogeny*
462 The GTR + G DNA substitution model was found to be optimal by the Bayesian
463 Information Criterion. The estimated ML tree (Fig. 3) contained two major clades, one
464 consisting of species infecting *M. buchanani* (Clade I) and the other consisting of species
465 infecting *L. subviridis* (Clade II), in agreement with observed host specificity. Bootstrap
466 support was high for most internal nodes, except the most recent common ancestor node of
467 *L. parvicopulatrix* and *L. bantingensis* (about 35%).
468
469 *Morphometry Summary Statistics*
470 Table S2 in Supplementary Material gives summary statistics of anchor size, anchor
471 shape, body size and male copulatory organ size for the 13 *Ligophorus* species.
472
473

Anchor Shape and Phylogeny Correlation

Scatter plots of GPA landmark configuration for each species are given in Figures S4-S16 in Supplementary Material. Figure 4 shows the PCA plots of PC2 against PC1, and PC3 against PC1 for shape variables of ventral and dorsal anchors (See Fig. S17 in Supplementary Material for a three-dimensional PCA plot). The first three PC accounted for 85% and 82% total shape variation in the ventral and dorsal anchors, respectively. To interpret these three PCs, we simultaneously compared the scatter plots of the GPA landmark configurations with the heat map of shape variable loadings (Fig. S18 and S19 in Supplementary Material). Anchors with a sickle-shaped shaft had large positive values of PC1 (e.g. ventral anchors of *L. fenestrum, L. grandis, L. kedahensis, L. johorensis*), while those with a scimitar-shaped shaft (e.g. ventral anchors of *L. chelatus, L. belanaki, L. navjotsodhii*) had large negative values in ventral anchors. For ventral anchors, large positive PC2 values were associated with V-shaped root grooves (e.g. *L. bantingensis*). In contrast, the U-shaped root groove (e.g. *L. liewi*, *L. kederai*) was associated with negative PC2 values. For dorsal anchors, PC2 was positive and large for highly symmetric inner and outer roots (e.g. *L. parvicopulatrix*) and vice versa (*L. liewi, L. bantingensis, L. grandis*). PC3 did not admit a simple geometrical interpretation.

The result of Adams's K-test supported the presence of significant phylogenetic signal in anchor shape (K = 1.015; p-value = 0.0001). Graphically, this is reflected in the PCA plots where both clades show divergent evolutionary trajectories in phylomorphospace (Fig. 4).

Cluster Analysis of Geometric Morphometric Data

The cluster heat map (Fig. 5) shows that variation in anchor shape alone allows the samples to be clustered unambiguously into 12 clusters corresponding to 12 of the

499 *Ligophorus* species, confirming that between species variation is much larger than within
500 species variation. On the other hand, with only eight specimens used, the clustering outcome
501 was ambiguous for *L. careyensis,* whose samples were variously clustered with those of *L.*
502 *funnelus*, *L. chelatus* and *L. belanaki*.

503 Consistent with the detection of significant phylogenetic signal in anchor shape,
504 hierarchical clustering revealed two major clades whose members were almost exactly the
505 same as those of Clade I and Clade II. An exception is *L. bantingensis*, which has the smallest
506 sized anchors. Its ventral anchor has a sickle-shaped shaft common to species in Clade I, but
507 V-shaped roots common to species in Clade II. Based on shape data, it was clustered in Clade
508 I, whereas it was clustered in Clade II based on host factor and DNA sequence data. The
509 quality of clustering using specimens that passed quality control was improved especially for
510 species with anchors that have very similar shapes such as *L. navjotsodhii* and *L. chelatus*.
511 The effect seems less remarkable for species that have anchors with larger shape differences,
512 such as those in Clade I, which were all completely clustered despite using specimens that
513 failed quality control.

514 For each shape variable, we labelled the samples according to their membership in
515 Clade I or Clade II, and then ranked the shape variables in descending order using the two-
516 sample t-statistic to reveal inverted block structures at the top and bottom of the heat map.
517 The shape variables that make up the top block come from the x-coordinates of LM2, LM3,
518 LM4, and y-coordinates of LM5, LM6, LM10, their values being relatively larger in species
519 belonging to Clade II compared to those in Clade I. The bottom block consists of shape
520 variables from the x-coordinates of LM6, LM8, LM10, LM11 and y-coordinates of LM1,
521 LM7, LM8, LM9. These values were relatively larger in species belonging to Clade I
522 compared to those in Clade II. Collectively, these variables suggest that the mean shape of
523 the anchor shaft in Clade II was more elongated and scimitar-like (i.e. LM5, LM6, LM10 and

LM7, LM8, LM9 are relatively farther from each other) while that in Clade I was more robust and sickle-like (i.e. LM5, LM6, LM10 and LM7, LM8, LM9 are relatively closer to each other).

Anchor Shape and Size Evolution

The wireframe-lollipop graphs (Fig. 6) show patterns of shape changes in the ventral and dorsal anchors of both clades that are consistent with those inferred from the cluster heat map and PCA. The circular plots (Fig. S20 and S21 in Supplementary Material) provide more details at the level of individual landmarks. The explicit visualization of the direction and magnitude of GPA-landmark coordinate deviation relative to the ancestral form provides insights into selection of new morphometric variables suitable as morphological characters. Specifically, for two landmarks, if their mean directional change is divergent in one clade but convergent in another, then the interlandmark distance is expected to be of value for discriminating the two clades. To be easy to measure, the landmarks should be of Type I. Thus, the distance from LM1 to LM3 and from LM1 to LM5 were found to be good candidates. We found the common practice of using the inner and outer root lengths (distance from LM1 to LM7 and LM3 to LM7, respectively) to be suboptimal since both LM1 and LM7 had almost parallel directional changes, whereas the mean magnitude of change in LM7 was too weak to be able to show large variation between Clade I and Clade II. Figure 7 (see also Fig. S22 and S23 in Supplementary Section) shows that it is possible to define cut-offs for the LM1-LM3 (15µm) and LM1-LM5 (25µm) distances that result in discrimination of Clade I from Clade I, but no reasonable cut-offs for the inner and outer lengths lead to similar results.

The average median body size of species in Clade I was significantly larger compared to Clade II (3.2 times; 95% confidence interval body size ratio = [1.5, 7]). However, larger

body size was not correlated with larger anchor size, after controlling for the effect of phylogeny (Ho-Ané phylogenetic regression p-values > 0.3). Consequently, both of them could be treated as independent covariates. Species in Clade I generally had larger anchors with sickle-shaped shaft (Fig. 8; ventral anchor mean = 170µm, standard deviation (SD) = 24 µm; dorsal anchor mean size = 165 µm, SD = 16 µm), whereas those in Clade II had smaller anchors (ventral anchor mean size = 140 µm, SD = 35 µm; dorsal anchor mean size = 133 µm, SD = 24 µm) with scimitar-shaped shaft. Size decrease was most striking in *L. bantingensis*, being 2.7 SD and 1.8 SD below the mean of all species for the ventral and dorsal anchors, respectively. Conversely, size increase was most prominent in *L. liewi*, with 1.7 SD above the mean of all species for both ventral and dorsal anchors. Nonetheless, the within clade trajectory for some species may sometimes show considerable variation from a clade's average trajectory. For example, *L. liewi* evolved a more slender shaft for its ventral and dorsal anchors, which is closer to the scimitar shape found in most species in Clade II, even though its anchor size was the largest. In contrast, *L. bantingensis* evolved sickle-shaped shafts in its ventral and dorsal anchors (common in Clade I species like *L. fenestrum* and *L. grandis*) even though it had the smallest anchor size.

Results from Adams-Collyer phylogenetic regression indicated that the interaction of body size and anchor size were not statistically significant in the dorsal anchor (p-values > 0.1), but anchor size was a significant predictor of anchor shape (p-value = 0.02). For the ventral anchor, interaction of body size and anchor size was a significant predictor of anchor shape (p-value = 0.02). Since body size and anchor shape were not significantly correlated, we may expect similar anchor shape to be found across a range of body sizes (Fig. S24 in Supplementary Material).

574

575 *Patterns of Morphometric and Morphological Variation in the Male Copulatory Organ and*
576 *Anchor*

577 Where the male copulatory organ was similar in size among closely-related species
578 with similar anchor shape and size, its morphology varied (I and II in Fig.9). *Ligophorus*
579 *belanaki*, *L. careyensis*, *L. navjotsodhii* and *L. chelatus* shared a most recent common
580 ancestor, whose ancestral character states for the three male copulatory organ characters
581 could be inferred as 113 on a parsimony criterion. The divergence of *L. careyensis* from *L.*
582 *belanaki* did not involve major changes in anchor shape, size and size of male copulatory
583 organ, but on the latter's morphology, which acquired three changes to become 002.
584 Similarly, The most recent common ancestor of *L. navjotsodhii* and *L. chelatus* probably
585 evolved character states 000 or 001 from 113, and divergence of these two species was
586 associated with a change in the third character state, with only relatively minor change in
587 either anchor shape, size or copulatory organ size.

588 In contrast, where the male copulatory organ was similar in morphology among
589 closely-related species with similar anchor shape and size, its size varied (III in Fig.9).
590 *Ligophorus kederai*, *L. grandis*, *L. kedahensis* and *L. johorensis* have similar anchor shape
591 and the same character states 114 for the morphology of their male copulatory organ.
592 Consistent with prediction from the Rohde-Hobbes hypothesis, substantial variation in the
593 size of their male copulatory organ was observed. It is possible for size and morphological
594 variation to co-occur in the male copulatory organ, as shown in the divergence of *L. grandis*
595 and *L. fenestrum* from their common ancestor.

596

597 *Morphological Integration*

The shapes of both ventral and dorsal anchors were strongly and significantly correlated (evolutionary correlation = 0.87, Adams-Felice test p-value < 0.001). Additionally, there was tight integration between the root and point compartments of the ventral (evolutionary correlation = 0.84, Adams-Felice test p-value = 0.003) and dorsal anchors (evolutionary correlation = 0.88, Adams-Felice test p-value = 0.001). Thus, the entire anchor can be considered as a single, fully integrated module. Across the ventral and dorsal anchors, integration of the point compartments was strong (evolutionary correlation = 0.92, Adams-Felice test p-value = 0.001) but that of the root compartments was weaker (evolutionary correlation = 0.74, Adams-Felice test p-value = 0.06). Figure S25 in Supplementary Material provides a graphical summary of the results of the morphological integration analysis.

Phylogenetically Informative Morphometric Variables

For the current 13 *Ligophorus* species, the maximum parsimony tree estimated using the set of morphological characters containing discretized LM1-LM3 and LM1-LM5 distances and anchor shape was better resolved (Fig. 10) . Clade I and Clade II were clearly identified, and the partially resolved relationships within each clade were also congruent with those of the molecular phylogeny's. In contrast, using morphological characters of anchors derived traditional morphometrics as in Sarabeev and Desdevises (2014) produced a maximum parsimony tree that was mostly reticulate and failed to distinguish Clade I and Clade II.

DISCUSSION

Data Quality Control

We are not aware of any geometric morphometric analyses of anchors in monogeneans that currently implement specimen quality control. Specimen quality

introduces an important source of non-biological variation into observed anchor shape variation, the impact of which depends on whether the data would be analyzed at the intra or interspecific level. Thus, while inclusion of specimens that failed quality control into hierarchical clustering did not fundamentally change species delimitation conclusion in this study, it is important to control for this confounder where intraspecific variation can be expected to impact conclusions of an analysis, for example, when investigating mean directional change in landmarks of anchors (Fig. 6), or testing for association between intraspecific anchor shape variation and evolutionary potential of a species (Rodríguez-González et al., 2015) . In the current study, we observed up to 50% loss of specimens (*L. fenestrum*) due to low quality score. Assuming this value optimistically as an upper bound, then at least 40 specimens per species would have to be obtained in order to anticipate at least 20 specimens that pass quality control. An ideal case like this may not always be possible, since sampling trips do not always yield sufficient study material.

Variation in quality scores can be attributed to several sources, such as the method of slide preparation, the quality of camera lens and software used for capturing images, and the skill and experience of the data gatherer. In this study, a single data gatherer (O.Y.M. Soo) prepared and acquired the landmark data, using the same compound microscope and computer. Because of this, we expect other factors to explain the poor quality scores. Interestingly, we note that species that had larger proportion of specimens failing quality control tend to have body and/or anchor size that were relatively large or small. In the case of *L. grandis* ($\log_{10}$ median body size 2.1 SD larger from total mean; dorsal anchor size 1.0 SD larger than total mean), *L. fenestrum* ($\log_{10}$ median body size 1.6 SD larger than total mean; dorsal anchor size 0.9 SD larger than total mean), and *L. bantingensis* ($\log_{10}$ median body size 0.9 SD smaller than total mean; ventral anchor size 2.7 SD smaller than total mean), we observed about 30%, 50% and 45% of the specimens failing quality control (Q-score < 10;

Fig. S2), respectively. A possible explanation may be that the robust anchors of *L. fenestrum* and *L. grandis* have uneven thickness at the root and point regions, which makes them difficult to evenly flatten on slides. The large body bulk may also further hinder effective flattening. Monogenean anchor thickness is not usually measured but may be indirectly inferred through 3D-modelling (Teo et al., 2010; Teo et al., 2013). Since size and physical inertia are positvely correlated, the small body and anchor size of *L. bantingensis* make specimen orientation on the slide sensitive to variation in force applied during slide flattening.

Phenotypic Plasticity in Anchor Shape

Different species were found to have varying levels of intraspecific phenotypic plasticity in this study. While within species shape variation in both ventral and dorsal anchors was large in some species (*L. kedahensis*, *L. parvicopulatrix*), it was limited in others (*L. grandis*, *L. liewi*). Interestingly, the generalist *L. bantingensis*, which has been reported to be found in two small fish hosts (Kritsky et al., 2013; FishBase Consortium, 2015): *Liza abu* (body length range: 12-15.5 cm) and *Liza klunzingeri* (body length range: 14-18cm), had the largest intraspecific shape variation in its ventral anchor, particularly in its root compartment (PC2). We tentatively assumed that the other 12 species were specialists as there are no other reports of them being found in hosts other than *M. buchanani* and *Liza subviridis*. Phenotypic plasticity within species likely promotes divergence by increasing the adaptability to different gill microhabitats (Pfennig et al., 2010), and is generally considered to be important for generalist species (van Valen, 1965).

Integrative Geometric Morphometric Analysis supports the Rohde-Hobbes Hypothesis

Evidence for supporting the Rohde-Hobbes Hypothesis has traditionally come from integrating spatial distribution data of monogeneans on gill microhabitats (e.g. Rohde, 1977; Ramasamy et al., 1985; Koskivaara et al., 1992) with morphological data of the monogenean species (e.g. Fig. 6.3 in Šimková and Rohde, 2013). These efforts were very laborious, but crucially established anchor shape-microhabitat association. Benefitting from such insights, our current integrative geometric morphometric analysis was able to reveal patterns consistent with the hypothesis's predictions on how male copulatory organ size and morphology vary with respect to anchor shape (Fig. 9), despite the absence of spatial distribution data for the 13 *Ligophorus* species across gill microhabitats.

Morphological Integration, Phylogenetic Signal and Morphological Phylogenetics

In their intraspecific study of morphological integration between the root and point compartments in *L. cephali*, Rodríguez-González et al. (2015) reported only modest degree of integration in the same anchor, but stronger compartmental integration between the ventral and dorsal anchors. On the other hand, using interspecific data, we demonstrated a much stronger degree of integration between the root and point compartments within anchors, and showed relatively weaker integration of root compartments between ventral and dorsal anchors. Intuitively, intraspecific compartmental integration within the same anchor is expected to be high, so a possible explanation for the discrepancy may be the lack of a quality control procedure for filtering poor quality slides. Without the latter, it seems difficult to rule out the possibility that the observed intraspecific anchor shape variation in *L. cephali* may contain non-trivial amount of artifactual noise.

Generally, a certain degree of homoplasy may be expected in the morphology of attachment organs in parasites, on grounds that functional requirements for attaching to the host and adapting to within-host microhabitats would override shape constraints imposed by

697 phylogeny (Morand et al., 2002). However, in this study we found phylogeny to be a major
698 determinant of anchor shape variation, in agreement with previous findings that sclerite
699 (including anchors) shape also present significant phylogenetic signal in *Cichlidogyrus*
700 (Vignon et al., 2011). The modest levels of anchor shape-size covariation revealed through
701 Adams-Collyer phylogenetic regression analysis suggest that, apart from the effect of shared
702 ancestry, anchor shape-size covariation is likely non-trivially constrained by additional
703 factors, one of which could be their biomechanical compatibility.
704
705 *Anchor Shape and Size Correlation with Host and Ecological Factors*
706 The patterns of evolution of anchor shape and size for the 13 *Ligophorus* species may
707 be associated with host size and ecology. On average, the larger *Moolgarda buchanani* (body
708 length range 35-48cm) harbored larger *Ligophorus* species, whereas the smaller *Liza*
709 *subviridis* (body length range 25-30cm) harbored smaller *Ligophorus* species. Sasal et al.
710 (1999) reported modest correlation between parasite body size and host body size in
711 specialists (R^2 ~ 30%).
712 The current analysis showed that *L. bantingensis* evolved anchors of a smaller size but
713 retained the sickle-shape shaft common in Clade I, which is associated with larger anchor
714 size. The observed small anchor size is consistent with the hypothesis that small or medium-
715 sized attachment organs are generally associated with a generalist lifestyle, as these sizes
716 expand the host range of monogeneans to small or medium-sized hosts, which are generally
717 more diversified than larger hosts (Morand et al., 2002).
718 There is circumstantial evidence suggesting that perhaps the larger and more robust
719 anchors in *Ligophorus* species infecting *M.buchanani* may be a consequence of the hosts'
720 adaptation to rough open seas, where strong water currents are expected. In the present study,
721 sampling in open seas (Langkawi Island) yielded only *M. buchanani* samples whereas

722 sampling in sheltered marine environment yielded both *M. buchanani* and *Liza subviridis*
723 samples. Thus, the U-shaped root groove in some species infecting *M. buchanani* (e.g. *L.*
724 *liewi*, *L. kederai* and *L. fenestrum*), which could result from the accretion of sclerotic material
725 in the space between the inner and outer root (Klaus Rohde, pers. comm., 2014), may have
726 substantially expanded the root base, providing space for connection with more muscle
727 tissues. This would likely have resulted in anchors with stronger contraction strength,
728 necessitating the evolution of the shorter but more robust sickle-shaped shaft, hence the
729 finding of tight morphological integration between the root and point compartments.
730 Interestingly, U-shaped roots and sickle-shaped shaft are also common in
731 *Cichlidogyrus* species (Vignon et al., 2011), which infect the cichlids in Africa. Ecologically,
732 it seems unlikely that such robust shapes would have evolved in freshwater environments,
733 where cichlids are mostly found. If the ancestors of cichlids and their monogenean parasites
734 were marine in origin, or host switching occurred with contact between salt-tolerant cichlids
735 and the marine ancestor of the monogenean parasite, the observed robust shapes would then
736 be inherited, with their shapes constrained by phylogeny. While some studies (Murray, 2001)
737 suggested that the ancestors of cichlids were likely marine, others were sceptical
738 (Chakrabarty, 2004; Sparks and Smith, 2005). Joint consideration of the morphology and
739 phylogeny of monogenean fauna of cichlids and other marine fishes is probably required
740 (Pariselle et al., 2011) to assess the competing claims. For example, a recent molecular
741 phylogenetic analysis using 28S rRNA sequence (Tan, 2013; Fig. S26 in Supplementary
742 Material) indicated that *Ligophorus* (marine) and *Cichlidogyrus* (mostly freshwater) species
743 shared the most recent common ancestor.
744 In three species (*L. grandis, L. funnelus* and *L. liewi*), fenestration in the anchor base
745 seems to be an invariant character state, as all examined specimens (n=22,50,32, respectively)
746 showed consistent presence of fenestration. Presently, the ecological significance of

747 fenestrations in anchors is unclear. Some progress may be possible with biomechanical
748 studies (e.g. Wong and Gorb, 2013) that compare whether fenestrated and non-fenestrated
749 anchors differ significantly in their resistance against turbulence and strong water currents.
750 The present phylogenetic analysis suggests that fenestration is not a synapomorphic character
751 state (Fig. 3), but a clearer picture requires more extensive taxa sampling.
752
753 *Outlook for Geometric Morphometric Analysis in Ligophorus*
754 Our present study used large numbers of samples, averaging about 35 per species.
755 Compared to laborious measuring of selected lengths as done in traditional morphometrics,
756 data acquisition is far more efficient with a landmark digitization software such as TPSDIG2,
757 which simultaneously captures shape and size variation information. This improved
758 efficiency is important – by greatly reducing the tedium associated with measuring many
759 lengths per specimen, there is more incentive to sample more extensively.
760 Although the geometric morphometric approach has been strongly advocated by
761 Vignon and Sasal (2010) as an effective means to pursue systematics research in
762 monogeneans, the scientific community still lack integrative tools that would make it easy to
763 share data and adopt a common analysis pipeline to ease comparison of old and new results.
764 Here, the `monogeneaGM` R package that we have developed enables substantial number of
765 shape and size variables from large number of samples to be analyzed efficiently to answer
766 multiple questions, ranging from systematic value of anchors to understanding patterns of
767 phenotypic and phylogenetic correlation in the *Ligophorus* genus. We hope the development
768 of `monogeneaGM` will contribute to reducing the bottleneck for large scale data analysis of
769 this genus. Indeed, as there has been a surge in systematic biology studies of *Ligophorus* in
770 recent years (Abdallah et al., 2009; Blasco-Costa et al., 2012; Dmitrieva et al., 2012, 2013;
771 Soo and Lim, 2012, 2015; El Hafidi et al., 2013; Kritsky et al., 2013; Ozer and Kirca, 2013;

Sarabeev and Desdevises, 2014; Soo et al., 2015), the analysis can only get more interesting as data from other species from other hosts in other geographical regions are added. We expect analysis tools in `monogeneaGM` to continue to evolve to handle complexities of data analysis when this happens.

The use of two-dimensional landmark data implies that analysis of anchor size and shape evolution is necessarily approximate, since some of the potential biological variation in anchor morphometry may only be adequately captured in three dimensions (Galli et al., 2007). Nevertheless, given the wealth of corroborative inference regarding anchor shape and size evolution that have been obtained in the current study, it appears that no general loss of interpretability arises from usage of two-dimensional data for geometric morphometric analysis in *Ligophorus*.

Future Prospects

While the use of genome-level data (Delsuc et al., 2005) may offer the potential of sampling sequence regions with strong phylogenetic signal, so that well-resolved phylogenies can be reliably inferred (Dunn et al., 2008; Johnson et al., 2010), adequate taxa coverage remains an important factor for accurate phylogenetic inference (Sanderson et al., 2010). The three markers used in this study are the most common ones reported for other known *Ligophorus* species in the GenBank database, hence their continued use supports efforts at expanding taxa sampling of molecular sequences. Indeed, a research program in *Ligophorus* systematics that expands taxa coverage of anchor geometric morphometric and sequence data opens up the possibility of using parasite phylogeny and anchor morphometry to test hypotheses of host genealogy and ecology (Nieberding and Olivieri, 2007) in grey mullets (Teleostei: Mugilidae), a speciose fish family that is economically important (Durand et al., 2012). Moreover, analysis of patterns of congruence between the phylogenies of the fish host

797 species and their *Ligophorus* parasites can provide insights into prevalence of host switching
798 (Zietara and Lumme, 2002) and thence the relative importance of allopatric and sympatric
799 speciation (Huyse et al., 2003) in shaping the diversity of this genus. It is also possible to
800 expand this analysis in a biogeographic context by sampling different geographical
801 populations of a host species, since some *Ligophorus* species have been reported to be useful
802 biological markers of geographical fish host populations (El Hafidi et al., 2013).
803
804 CONCLUSION
805 The presence of significant phylogenetic signal in the anchor makes the quantitative
806 analysis of its shape and size variables useful in answering species delimitation and
807 evolutionary problems in the *Ligophorus* genus, and potentially, in other monogenean genera
808 as well. In this study, we inferred two major host-specific clades from DNA sequence data,
809 which corroborated well with clades inferred from geometric morphometric data from
810 anchors. We further extracted size information through the first principal of size variables
811 based on all pairwise Euclidean distances between landmarks, and showed that *Ligophorus*
812 species infecting *Moolgarda buchanani* generally evolved larger anchors compared to those
813 infecting *Liza subviridis*. Anchor shape was correlated with anchor size after controlling for
814 the effect of phylogeny. Subsequently, through analysis of directional change, we discovered
815 two new morphological characters based on the length between inner and outer root tips and
816 the length between inner root tip and the groove point, which proved more phylogenetically
817 informative than existing characters based on the inner and outer lengths. Finally, we
818 demonstrated evidence for significant interspecific morphological integration of the root and
819 point compartments within anchors, as well as integration of the same compartment between
820 ventral and dorsal anchors.
821

SOFTWARE AVAILABILITY

The `monogeneaGM` package is available for download at https://cran.r-project.org/web/packages/monogeneaGM/. Analyses in this study can be replicated using the R scripts deposited in GitHub (http://github.com/tfkhang/monogenea).

SUPPLEMENTARY MATERIAL

Data and additional figures available from the Dryad Digital Repository at http://dx.doi.org/10.5061/dryad.xxxx

FUNDING

This work was supported by University of Malaya Research Grant RG 197/12SUS to TFK and LHSL, and RP004D-13SUS to LHSL, WBT and TFK.

ACKNOWLEDGMENTS

This work is dedicated to the memory of Lee Hong Susan Lim (1952-2014), who conceived the present project. Susan Lim contributed actively to global monogenean systematics for decades, and was instrumental at developing and transmitting this art in Malaysia. Klaus Rohde read the manuscript and provided helpful feedback. We thank Thian Liang Cheow for contributing R codes for data processing.

REFERENCES

845 Abdallah V.D., de Azevedo R.K., Luque J.L. 2009. Four new species of *Ligophorus*
846 (Monogenea: Dactylogyridae) parasitic on *Mugil liza* (Actinopterygii: Mugilidae) from
847 Guandu River, southeastern Brazil. J. Parasitol. 95: 855-864.

848 Adams D.C. 2014a. A generalized K statistic for estimating phylogenetic signal from shape
849 and other high-dimensional data. Syst. Biol. 63: 685-697.

850 Adams D.C. 2014b. A method for assessing phylogenetic least squares models for shape and
851 other high-dimensional multivariate data. Evolution 68: 2675-2688.

852 Adams D.C., Felice R.N. 2014. Assessing trait covariation and morphological integration on
853 phylogenies using evolutionary covariance matrices. PLoS ONE 9(4): e94335.

854 Adams D.C., Otarola-Castillo E. 2013. geomorph: an R package for the collection and
855 analysis of geometric morphometric shape data. Methods Ecol. Evol. 4: 393-399.

856 Adams D.C., Rohlf F.J., Slice D.E. 2004. Geometric morphometrics: ten years of progress
857 following the “revolution”. Ital. J. Zool. 71: 5-16.

858 Adams D.C., Rohlf F.J., Slice D.E. 2013. A field comes of age: geometric morphometrics in
859 the 21st century. Hystrix 24: 7-14.

860 Adler D., Murdoch D., et al. 2014. rgl: 3D visualization device system (OpenGL). R package
861 version 0.95.1201. Available at http://CRAN.R-project.org/package=rgl.

862 Agostinelli C., Lund U. 2013. R package 'circular': Circular Statistics (version 0.4-7).
863 Available at:https://r-forge.r-project.org/projects/circular.

864 Arnqvist G., Mårtensson T. 1998. Measurement error in geometric morphometrics: empirical
865 strategies to assess and reduce its impact on measures of shape. Acta Zool. Acad. Sci. H. 44:
866 73-96.

867 Barão K.R., Gonçalves G.L., Mielke O.H.H., Kronforst M.R., Moreira G.R.P. 2014. Species
868 boundaries in *Philaethria* butterflies: an integrative taxonomic analysis based on genitalia
869 ultrastructure, wing geometric morphometrics, DNA sequences, and amplified fragment
870 length polymorphisms. Zool. J. Linn. Soc. 170: 690-709.

871 Batagelj V. 1988. Generalized Ward and related clustering problems. In: Bock H.H., editor.
872 Classification and Related Methods of Data Analysis. Amsterdam: North-Holland. p. 67-74.

873 Batschelet E. 1981. Circular Statistics in Biology. London: Academic Press.

874 Blasco-Costa I., Miguez-Lozano R., Balbuena J.A. 2012. Molecular phylogeny of species of
875 *Ligophorus* (Monogenea: Dactylogyridae) and their affinities within the Dactylogyridae.
876 Parasitol. Int. 61: 619-627.

877 Chakarabarty P. 2004. Cichlid biogeography: comment and review. Fish Fish. 5: 97-119.

878 Collyer M.L., Sekora D.J., Adams D.C. 2014. A method for analysis of phenotypic change
879 for phenotypes described by high-dimensional data. Heredity doi:10.1038/hdy.2014.75.

880 Conesa M.A., Mus M., Rosselló J.A. 2012. Leaf shape variation and taxonomic boundaries in
881 two sympatric rupicolous species of *Helichrysum* (Asteraceae: Gnaphalidae), assessed by
882 linear measurements and geometric morphometry. Biol. J. Linn. Soc. 106: 498-513.

883 Cruz R.A.L., Pante M.J.R., Rohlf F.J. 2012. Geometric morphometric analysis of shape
884 variation in *Conus* (Gastropoda: Conidae). Zool. J. Linn. Soc. 165: 296-310.

885 De Meeus T., Michalakis Y., Renaud F. 1998. Santa Rosalia revisited: or why are there so
886 many kinds of parasites in 'The Gardern of Earthly Delights'? Parasitol. Today 14: 10-13.

887 Delsuc F., Brinkmann H., Philippe H. 2005. Phylogenomics and the reconstruction of the tree
888 of life. Nature Rev. Genet. 6: 361-375.

889 Dmitrieva E.V., Gerasev P.I., Gibson D.I., Pronkina N.V., Galli P. 2012. Descriptions of
890 eight new species of *Ligophorus* Euzet & Suriano, 1977 (Monogenea: Ancyrocephalidae)
891 from Red Sea mullets. Syst. Parasitol. 81: 203-237.

892 Dmitrieva E.V., Gerasev P.I., Gibson D.I. 2013. *Ligophorus abditus* n. sp. (Monogenea:
893 Ancyrocephalidae) and other species of *Ligophorus* Euzet & Suriano, 1977 infecting the
894 flathead grey mullet *Mugil cephalus* L. in the Sea of Japan and the Yellow Sea. Syst.
895 Parasitol. 85: 117-130.

896 Dunn C.W., Hejnol A., Matus D.Q., Pang K., Browne W.E., Smith S.A., Seaver E., Rouse
897 G.W., Obst M., Edgecombe G.D., Sorensen M.V., Haddock H.D., Schmidt-Rhaesa A., Okusu
898 A., Kristensen R.M., Wheeler W.C., Martindale M.Q., Giribet G. 2008. Broad phylogenomic
899 sampling improves resolution of the animal tree of life. Nature 452: 745-749.

900 Durand J.D., Shen K.N., Chen W.J., Jamandre B.W., Blel H., Diop K., Nirchio M., Garcia de
901 Leon F.H., Whitfield A.K., Chang C.W., Borsa P. 2012. Systematics of the grey mullets
902 (Teleostei: Mugiliformes: Mugilidae): molecular phylogenetic evidence challenges two
903 centuries of morphology-based taxonomy. Mol. Phylogenet. Evol. 64: 73-92.

904 El Hafidi F., Rkhami O.B., de Buron I., Durand J-D., Pariselle A. 2013. *Ligophorus* species
905 (Monogenea: Ancyrocephalidae) from *Mugil cephalus* (Teleostei: Mugilidae) off Morocco
906 with the description of a new species and remarks about the use of *Ligophorus* spp. as
907 biological markers of host populations. Folia Parasitol. 60: 433-440.

908 Felsenstein J. 1981. Evolutionary trees from DNA sequences: a maximum likelihood
909 approach. J. Mol. Evol. 17: 368-376.

910 Felsenstein J. 2003. Inferring Phylogenies. Sunderland, MA: Sinaeur Associates.

FishBase Consortium. 2015. FishBase: A global information system on fishes. Available at http://fishbase.org. Accessed 15 June 2015.

Galli P., Strona G., Villa A.M., Benzoni F., Stefani F., Doglia S.M., Kritsky D.C. 2006. Two-dimensional versus three-dimensional morphometry of monogenoidean sclerites. Int. J. Parasitol. 37: 449-456.

Gower J.C. 1975. Generalized procrustes analysis. Psychometrika 40: 33-51.

Hahn C., Bakke T.A., Bachmann L., Weiss S., Harris P.D. 2011. Morphometric and molecular characterization of *Gyrodactylus teuchis* Lautraite, Blanc, Thiery, Daniel & Vigneulle, 1999 (Monogenea: Gyrodactylidae) from an Austrian brown trout population. Parasitol. Int. 60: 480-487.

Hayward C. 2005. Monogenea Polyopisthocotylea (ectoparasitic flukes). In: Rohde K., editor. Marine Parasitology. Australia: CSIRO Publishing. p. 55-63.

Ho L.S.T., Ané C. 2014. A linear-time algorithm for Gaussian and non-Gaussian trait evolution models. Syst. Biol. 63: 397-408.

Huyse T., Audenaert V., Volckaert F.A.M. 2003. Speciation and host-parasite relationships in the parasite genus *Gyrodactylus* (Monogenea, Platyhelminthes) infecting gobies of the genus *Pomatoschistus* (Gobiidae, Teleostei). Int. J. Parasitol. 33: 1679-1689.

Huyse T., Volckaert F.A. 2005. Comparing host and parasite phylogenies: *Gyrodactylus* flatworms jumping from goby to goby. Syst. Biol. 54: 710-718.

Jarkovský J., Morand S., Šimková A., Gelnar M. 2004. Reproductive barriers between congeneric monogenean parasites (*Dactylogyrus*: Monogenea): attachment apparatus morphology or copulatory organ incompatibility? Parasitol. Res. 92: 95-105.

933 Johnson B.R., Borowiec M.L., Chiu J.C., Lee E.K., Atallah J., Ward P.S. 2010.
934 Phylogenomics resolves evolutionary relationships among ants, bees, and wasps. Curr. Biol.
935 23: 2058-2062.

936 Jolliffe I.T. 2002. Principal Component Analysis. 2nd ed. New York: Springer-Verlag.

937 Kahle D., Wickham H. 2013. ggmap: spatial visualization with ggplot2. The R Journal 5(1):
938 144-161.

939 Katoh K., Standley D.M. 2013. MAFFT multiple sequence alignment software version 7:
940 Improvements in performance and usability. Mol. Biol. Evol. 30: 772-780.

941 Khang T.F. 2015. monogeneaGM: geometric morphometric analysis of monogenean anchors.
942 R package version 1.0. Available at: http://CRAN.R-project.org/package=monogeneaGM.

943 Klingenberg C.P. 2008. Morphological integration and developmental modularity. Annu.
944 Rev. Ecol. Evol. Syst. 39: 115-132.

945 Klingenberg C.P. 2013. Visualizations in geometric morphometrics: how to read and how to
946 make graphs showing shape changes. Hystrix 24:15–24.

947 Klingenberg C.P., Ekau W. 1996. A combined morphometric and phylogenetic analysis of an
948 ecomorphological trend: pelagization in Antarctic fishes (Perciformes: Nototheniidae). Biol.
949 J. Linn. Soc. 59: 143-177.

950 Koskivaara M., Valtonen E.T., Vuori K-M. 1992. Microhabitat distribution and coexistence
951 of *Dactylogyrus* species (Monogenea) on the gills of roach. Parasitology 104: 273-281.

952 Kritsky D.C., Khamees N.R., Ali A.H. 2013. *Ligophorus* spp. (Monogenoidea:
953 Dactylogyridae) parasitizing mullets (Teleostei: Mugiliformes: Mugilidae) occurring in the
954 fresh and brackish waters of the Shatt Al-Arab River and Estuary in southern Iraq, with the

description of *Ligophorus sagmarius* sp. n. from the greenback mullet *Chelon subviridis* (Valenciennes). Parasitol. Res. 112: 4029-4041.

Lambert A., Maillard C. 1975. Repartition branchiale de deux monogenes: *Diplectanum aequans* (Wagener, 1857) Diesing, 1858 et *D. laubieri* Lambert A., Maillard, C., 1974 (Monogenea: Monopisthocotylea) parasites simultanes de *Dicentrarchus labrax* (Teleosteen). Ann. Parasitol. Hum. Comp. 50: 691-699.

Lim L.H.S. 1991. Three new species of *Bychowskyella* Achmerow, 1952 (Monogenea) from Peninsular Malaysia. Syst. Parasitol. 19: 33-41.

Lim L.H.S., Gibson D.I. 2009. A new monogenean genus from an ephippid fish off Peninsular Malaysia. Syst. Parasitol. 73: 13-25.

Littlewood D.T.J., Olson P.D. 2001. Small subunit rDNA and the Platyhelminthes: Signal, noise, conflict and compromise. In: Littlewood D.T.J., Bray R.A., editors. Interrelationships of the Platyhelminthes. New York: Taylor & Francis. p. 262-278.

MacLeod N. 2013. Landmarks and semilandmarks: differences without meaning and meaning without differences. Available at: http://www.palass.org.

Maddison W.P. 1997. Gene trees in species trees. Syst. Biol. 46: 523-536.

Marcus L.F. 1990. Traditional morphometrics. In: Rohlf F.J., Bookstein F.L., editors. Proceedings of the Michigan Morphometrics Workshop. Ann Arbor, Michigan: University of Michigan Museums. p.77-122.

Mariniello L., Ortis M., D'Amelio S., Petrarca V. 2004. Morphometric variability between and within species of *Ligophorus* Euzet & Suriano, 1977 (Monogenea: Ancyrocephalidae) in the Mediterranean Sea. Syst. Parasitol. 57: 183-190.

977 Mendlová M., Šimková A. 2014. Evolution of host specificity in monogeneans parasitizing
978 African cichlid fish. Parasit. Vectors 7: 69.

979 Morand S., Šimková A., Matejusová I., Plaisance L., Verneau O., Desdevises Y. 2002.
980 Investigating patterns may reveal processes: evolutionary ecology of ectoparasitic
981 monogeneans. Int. J. Parasitol. 32: 111-119.

982 Mouillot D., Šimková A., Morand S., Poulin R. 2005. Parasite species coexistence and
983 limiting similarity: a multiscale look at phylogenetic, functional and reproductive distances.
984 Oecologia 146: 269-278.

985 Mundry R. 2014. Statistical issues and assumptions of phylogenetic generalized least squares.
986 In: Garamszegi L.Z., editor. Modern Phylogenetic Comparative Methods and Their
987 Application in Evolutionary Biology. New York: Springer-Verlag. p. 131-153.

988 Murray A.M. 2001. The fossil record and biogeography of the Cichlidae (Actinopterygii:
989 Labroidei). Biol. J. Linn. Soc. 74: 517-532.

990 Nieberding C.M., Olivieri I. 2007. Parasites: proxies for host genealogy and ecology? Trends
991 Ecol. Evol. 22: 156-165.

992 Olson E.C., Miller E.L. 1958. Morphological Integration. Chicago: University of Chicago
993 Press.

994 Ozer A., Kirca D. 2013. Parasite fauna of Golden Grey Mullet *Liza aurata* (Risso, 1810)
995 collected from Lower Kizilirmak Delta in Samsun, Turkey. Helminthologia 50: 269-280.

996 Paradis E., Claude J., Strimmer K. 2004. APE: Analyses of Phylogenetics and Evolution in R
997 language. Bioinformatics 20: 289-290.

998 Pariselle A., Boeger W.A., Snoeks J., Bilong Bilong C.F., Morand S., Vanhove M.P.M. 2011.
999 The monogenean parasite fauna of cichlids: a potential tool for host biogeography. Int. J.
1000 Evol. Biol. 2011: 471480.

1001 Perkins E.M., Donnellan S.C., Bertozzi T., Chisholm L.A., Whittington I.D. 2009. Looks can
1002 deceive: molecular phylogeny of a family of flatworm ectoparasites (Monogenea:
1003 Capsalidae) does not reflect current morphological classification. Mol. Phylogenet. Evol. 52:
1004 705-714.

1005 Pepinelli M., Spironello M., Currie D.C. 2013. Geometric morphometrics as a tool for
1006 interpreting evolutionary transitions in the black fly wing (Diptera: Simuliidae). Zool. J. Linn.
1007 Soc. 169: 377-388.

1008 Pérez Ben C.M., Gómez R.O., Báez A.M. 2014. Intraspecific morphological variation and its
1009 implication in the taxonomic status of '*Bufo pisanoi*', a Pliocene anuran from eastern
1010 Argentina. J. Vertebr. Paleontol. 34: 767-777.

1011 Pfennig D.W., Wund M.A., Snell-Rood E.C., Cruickshank T., Schlichting C.D., Moczek A.P.
1012 2010. Phenotypic plasticity's impacts on diversification and speciation. Trends Ecol. Evol.
1013 25: 459-467.

1014 Pizzo A., Zagaria D., Palestrini C. 2013. An unfinished speciation process revealed by
1015 geometric morphometrics, horn allometries and biomolecular analyses: The case of the
1016 fracticornis-similis-opacicollis species complex of the genus *Onthophagus* (Coleoptera:
1017 Scarabaeidae). Zool. Anz. 252: 548-561.

1018 Poisot T., Desdevises Y. 2010. Putative speciation events in *Lamellodiscus* (Monogenea:
1019 Diplectanidae) assessed by a morphometric approach. Biol. J. Linn. Soc. 99: 559-569.

1020 Poulin R. 2002. The evolution of monogenean diversity. Int. J. Parasitol. 32: 245-254.

1021 R Core Team. 2014. R: A language and environment for statistical computing. R Foundation
1022 for Statistical Computing. Vienna, Austria. URL http://www/R-project.org/.

1023 Rae T.C. 1998. The logical basis for the use of continuous characters in phylogenetic
1024 systematics. Cladistics 14: 221-228.

1025 Ramasamy P., Ramalingam K., Hanna R.E.B., Halton D.W. 1985. Microhabitat of gill
1026 parasites (Monogenea and Copepoda) of teleosts (*Scomberoides* spp.). Int. J. Parasitol. 15:
1027 385-397.

1028 Reyment R.A., Blackith R.E., Campbell N.A. 1984. Multivariate Morphometrics. 2nd ed.
1029 London: Academic Press.

1030 Revell L.J. 2012. phytools: an R package for phylogenetic comparative biology (and other
1031 things). Methods Ecol. Evol. 3: 217-223.

1032 Revell L.J. 2014. Graphical methods for visualizing comparative data on phylogenies. In:
1033 Garamszegi L.Z., editor. Modern Phylogenetic Comparative Methods and Their Application
1034 in Evolutionary Biology. New York: Springer-Verlag. p. 77-104.

1035 Rodríguez-González A., Míguez-Lozano R., Llopis-Belenguer C., Balbuena J.A. 2015.
1036 Phenotypic plasticity in haptoral structures of *Ligophorus cephali* (Monogenea:
1037 Dactylogyridae) on the flathead mullet (*Mugil cephalus*): a geometric morphometric
1038 approach. Int. J. Parasitol. 45: 295-303.

1039 Rohde K. 1977. A non-competitive mechanism responsible for restricting niches. Zool. Anz.
1040 199: 164-172.

1041 Rohde K. 1979. A critical evalution of intrinsic and extrinsic factors responsible for niche
1042 restriction in parasites. Am. Nat. 114: 648-671.

1043 Rohde K. 1994. Niche restriction in parasites – proximate and ultimate causes. Parasitology
1044 109: S69-S84.

1045 Rohde K., Hobbs R.P. 1986. Species segregation: competition or reinforcement of
1046 reproductive barriers? In: Cremin M., Dobson C., Noorhouse E., editors. Parasites Lives:
1047 Papers on Parasites, Their Hosts and Their Associations to Honour JFA Sprent. St. Lucia:
1048 University of Queensland Press. p.189-199.

1049 Rohde K., Hayward C., Heap M., Gosper D. (1994). A tropical assemblage of ectoparasites –
1050 gill and head parasites of *Lethrinus miniatus* (Teleostei, Lethrinidae). Int. J. Parasitol. 24:
1051 1031-1053.

1052 Rohlf F.J. 2013. tpsDig, digitize landmarks and outliers, version 2.17. Department of Ecology
1053 and Evolution, State University of New York at Stony Brook.

1054 Rohlf F.J. 2015. The tps series of software. Hystrix. 26, doi: 10.4404/hystrix-26.1-11264.

1055 Rohlf F.J., Corti M. 2000. Use of two-block partial least-squares to study covariation in
1056 shape. Syst. Biol. 49: 740-753.

1057 Rohlf F.J., Marcus L.F. 1993. A revolution in morphometrics. Trends Ecol. Evol. 8: 129-132.

1058 Rohlf F.J., Slice D.E. 1990. Extensions of the Procrustes method for the optimal
1059 superimposition of landmarks. Syst. Zool. 39: 40-59.

1060 Roubal F.R. 1981. The taxonomy and site specificity of the metazoan ectoparasites on the
1061 black bream, *Acanthopagrus australis* (Günther), in northern New South Wales. Aust. J.
1062 Zool. 30: 1-100.

1063 Sanderson M.J., McMahon M.M., Steel M. 2010. Phylogenomics with incomplete taxon
1064 coverage: the limits to inference. BMC Evol. Biol. 10:155.

1065 Sarabeev V., Desdevises Y. 2014. Phylogeny of the Atlantic and Pacific species of
1066 *Ligophorus* (Monogenea: Dactylogyridae): morphology vs. molecules. Parasitol. Int. 63: 9-
1067 20.

1068 Sasal P., Trouvé S., Müller-Graf C., Morand S. 1999. Specificity and host predictability: a
1069 comparative analysis among monogenean parasites of fish. J. Anim. Ecol. 68: 437-444.

1070 Shinn A.P., Gibson D.I., Sommerville C. 2001. Morphometric discrimination of
1071 *Gyrodactylus salaris* Malmberg (Monogenea) from species of *Gyrodactylus* parasitizing
1072 British salmonids using novel parameters. J. Fish Dis. 24: 83-97.

1073 Shinn A.P., Hansen H., Olstad K., Bachmann L., Bakke T.A. 2004. The use of morphometric
1074 characters to discriminate specimens of laboratory-reared and wild populations of
1075 *Gyrodactylus salaris* and *G. thymali* (Monogenea). Folia Parasitol. 51: 239:252.

1076 Sidlauskas B. 2008. Continuous and arrested morphological diversification in sister clades of
1077 characiform fishes: a phylomorphospace approach. Evolution 12: 3135-3156.

1078 Sidlauskas B.L., Mol J.H., Vari R.P. 2011. Dealing with allometry in linear and geometric
1079 morphometrics: a taxonomic case study in the *Leporinus cylindriformis* group
1080 (Characiformes: Anostomidae) with description of a new species from Suriname. Zool. J.
1081 Linn. Soc. 162: 103-130.

1082 Sievwright H., Macleod N. 2012. Eigensurface analysis, ecology, and modelling of
1083 morphological adaptation in the falconiform humerus (Falconiformes: Aves). Zool. J. Linn.
1084 Soc. 165: 390-419.

1085 Šimková A., Morand S. 2008. Co-evolutionary patterns in congeneric monogeneans: a review
1086 of *Dactylogyrus* species and their cyprinid hosts. J. Fish Biol. 73: 2210-2227.

1087

Šimková A., Rohde K. 2013. Community stability and instability in ectoparasites of marine and freshwater fish. In: Rohde K., editor. The Balance of Nature and Human Impact. Cambridge: Cambridge University Press. p. 75-88.

Šimková A., Ondračková M., Gelnar M., Morand S. 2002. Morphology and coexistence of congeneric ectoparasite species: reinforcement of reproductive isolation? Biol. J. Linn. Soc. 76: 125–135.

Šimková A., Verneau O., Gelnar M., Morand S. 2006. Specificity and specialization of congeneric monogeneans parazitizing cyprinid fish. Evolution 60: 1023–1037.

Smith U.E., Hendricks J.R. 2013. Geometric morphometric character suites as phylogenetic data: extracting phylogenetic signal from gastropod shells. Syst. Biol. 62: 366-385.

Soo O.Y.M., Lim L.H.S. 2012. Eight new species of *Ligophorus* Euzet & Suriano, 1977 (Monogenea: Ancyrocephalidae) from mugilids off Peninsular Malaysia. Raffles Bull. Zool. 60: 241-264.

Soo O.Y.M., Lim L.H.S. 2015. A description of two new species of *Ligophorus* Euzet & Suriano, 1977 (Monogenea: Ancyrocephalidae) from Malaysian mugilid fish using principal component analysis and numerical taxonomy. J. Helminthol. 89: 131-149.

Soo O.Y.M., Tan W.B., Lim L.H.S. 2015. Three new species of *Ligophorus* Euzet & Suriano, 1977 (Monogenea: Ancyrocephalidae) from *Moolgarda buchanani* (Bleeker) off Johor, Malaysia based on morphological, morphometric and molecular data. Raffles Bull. Zool. 63: 49-65.

Sparks J.S., Smith W.L. 2005. Freshwater fishes, dispersal ability, and non-evidence: "Gondwana Life Rafts" to the rescue. Syst. Biol. 53: 11-19.

1110 Swofford D.L. 2002. PAUP: phylogenetic analysis using parsimony, Ver. 4.0.b10.
1111 Sunderland, Massachusetts: Sinaeur Associates.

1112 Tamura K., Stecher G., Pedersen D., Filipski A., Kumar S. 2013. MEGA 6: Molecular
1113 Evolutionary Genetics Analysis Version 6.0. Mol. Biol. Evol. 30: 2725-2729.

1114 Tan W.B. 2013. Morphological and molecular characterisation of monogeneans. Ph.D thesis,
1115 University of Malaya.

1116 Tan W.B., Khang T.F., Lim L.H.S. 2010. Morphometric analysis of *Trianchoratus* Price &
1117 Berry, 1966 (Monogenea: Heteronchocleidinae) from *Channa* spp. (Osteichthyes: Channidae)
1118 of Peninsular Malaysia. Raffles Bull. Zool. 58: 165-172.

1119 Teo B.G., Sarinder K.K.S., Lim L.H.S. 2010. A novel alternative method for 3D visualisation
1120 in parasitology: the construction of a 3D model of a parasite from 2D illustrations. Trop.
1121 Biomed. 27: 254-264.

1122 Teo B.G., Sarinder K.K.S., Lim L.H.S. 2013. A deformable generic 3D model of haptoral
1123 anchor of monogenean. PLoS ONE 8(10): e77650.

1124 Thiele K. 1993. The holy grail of the perfect character: the cladistic treatment of
1125 morphometric data. Cladistics 9: 275-304.

1126 van Valen L. 1965. Morphological variation and width of ecological niche. Am. Nat. 99: 377-
1127 390.

1128 Vignon M. 2011. Putting in shape – towards a unified approach for the taxonomic description
1129 of monogenean haptoral hard parts. Syst. Parasitol. 79: 161-174.

1130 Vignon M., Sasal P. 2010. The use of geometric morphometrics in understanding shape
1131 variability of sclerotized haptoral structures of monogeneans (Platyhelminthes) with insights
1132 into biogeographic variability. Parasitol. Int. 59: 183-191.

1133 Vignon M., Pariselle A., Vanhove M.P.M. 2011. Modularity in attachment organs of African
1134 *Cichlidogyrus* (Platyhelminthes: Monogenea: Ancyrocephalidae) reflects phylogeny rather
1135 than host specificity or geographic distribution. Biol. J. Linn. Soc. 102: 694-706.

1136 Warnes G.R., Bolker B., Bonebakker L., Gentleman R., Huber W., Liaw A., Lumley T.,
1137 Maechler M., Magnusson A., Moeller S., Scharwtz M., Venables B. 2014. gplots: various R
1138 programming tools for plotting data. R package version 2.13.0. Available at: http://CRAN.R-
1139 project.org/pacakge=gplots.

1140 Werneburg I., Wilson L.A.B., Parr W.C.H., Joyce W.G. 2015. Evolution of neck vertebral
1141 shape and neck retraction at the transition to modern turtles: an integrated geometric
1142 morphometric approach. Syst. Biol. 64: 187-204.

1143 Wheeler Q.D. 2007. Digital innovation and taxonomy's finest hour. In: Macleod N., editor.
1144 Automated Taxon Identification in Systematics: Theory, Approaches and Applications. Boca
1145 Raton: CRC Press. p. 9-23.

1146 Whittington I.D. 2005. Monogenea Monopisthocotylea (ectoparasitic flukes). In: Rohde K.,
1147 editor. Marine Parasitology. Australia: CSIRO Publishing. p. 63-72.

1148 Whittington I.D., Cribb B.W., Hamwood T.E., Halliday J.A. 2000. Host-specificity of
1149 monogenean (platyhelminth) parasites: a role for anterior adhesive areas? Int. J. Parasitol. 30:
1150 305-320.

1151 Wiens J.J. 2001. Character analysis in morphological phylogenetics: problems and solutions.
1152 Syst. Biol. 50: 689-699.

1153 Wilkinson L., Friendly M. 2008. The history of the cluster heat map. Am. Stat. 63: 179-184.

1154 Wong W.L., Gorb S.N. 2013. Attachment ability of a clamp-bearing fish parasite, *Diplozoon*
1155 *paradoxum* (Monogenea) on gills of the common bream *Abramis brama*. J. Exp. Biol. 216:
1156 3008-3014.

1157 Zietara M.S., Lumme J. 2002. Speciation by host switch and adaptive radiation in a fish
1158 parasite genus *Gyrodactylus* (Monogenea, Gyrodactylidae). Evolution 56: 2445-2458.

1159

1160 FIGURE CAPTIONS

1161 FIGURE 1. a) Landmarks of the i) ventral and ii) dorsal anchors of a *L. navjotsodhii* sample,
1162 digitized using TPSDIG2 (Version 2.17). The iii) ventral and iv) dorsal bars can also be seen
1163 in the image. b) Landmark positions on an anchor. Type I landmarks
1164 (LM1,LM2,LM3,LM5,LM7,LM8) are indicated by stars, while Type III landmarks
1165 (LM4,LM6,LM9,LM10,LM11) are indicated by solid circles. Abbreviations: ORP - outer
1166 root point; GP - groove point; IRP - inner root point; DP - dent point; CP - curve point; TP -
1167 tip point.

1168 FIGURE 2. Wireframe plots of anchors of *L. bantingensis* lying in their natural positions in
1169 the mounted slide. a) Example of a poor quality specimen (Q = 1); note substantial variation
1170 between shape of (larger) left and right forms of the dorsal anchors, which shows up in a
1171 Tukey Mean Difference (TMD) plot that has relatively wide width of 95% limits of
1172 agreement (upper and lower dashed lines) as well as a fanning pattern as *A* becomes larger. b)
1173 Example of a good quality specimen (Q=40); note lack of shape variation between left and
1174 right forms of ventral and dorsal anchors, which shows up in a TMD plot with much

narrower width of 95% limits of agreement as well as a more or less random deviation of *M* about 0 independent of *A*.

FIGURE 3. Molecular phylogeny of the 13 *Ligophorus* species inferred using the maximum likelihood method (500 bootstrap replicates) with annotations from three anatomical structures: anchors, bars and male copulatory organ (30% of original scale). Species in Clade I are found in *Moolgarda buchanani*, and species in Clade II are found in *Liza subviridis*. The ventral and dorsal forms of the anchors are arranged from left to right, those of the bars from top to bottom.

FIGURE 4. PCA plots of PC1 against PC2 and PC3 for a) ventral and b) dorsal anchors, with superimposed phylogeny of the 13 *Ligophorus* species. The centroids of the species are indicated in solid colors, while individual samples are plotted in high transparency colors. The estimated principal component coordinates of the ancestral nodes are represented by small open circles.

FIGURE 5. Cluster heat map of specimens (column) using shape variable data (row). The name of a shape variables consists of three parts: a prefix indicating ventral (V) or dorsal (D) anchors, a number indicating landmark index, and a suffix indicating x or y coordinate value. a) Cluster heat map using filtered specimens with quality score of 10 or more (n=443); b) Cluster heat map using all specimens (n=537).

FIGURE 6. Wireframe-lollipop plots of mean shape change relative to estimated ancestral mean shape in a) ventral anchors of Clade I (purple); b) dorsal anchors of Clade I; c) ventral anchors of Clade II (blue); d) dorsal anchors of Clade II. The p-value of Rayleigh test for uniform direction change at each landmark is indicated as a colored solid circle. The color bar maps color tones to their corresponding p-values.

FIGURE 7. Scatter plots LM1-LM5 distance against LM1-LM3 distance for a) ventral and b) dorsal anchors. The dashed lines are cut-offs on the x and y axes that allow complete discrimination of Clade I from Clade II. Scatter plots of outer length (OL) against inner length (IL) for c) ventral and d) dorsal anchors. No cut-offs on the x and y axes permit complete discrimination of Clade I from Clade II.

FIGURE 8. Continuous character mapping of anchor size (in μm) of ventral (left) and dorsal (right) anchors onto the maximum likelihood phylogeny of the 13 *Ligophorus* species.

FIGURE 9. Scatter plot of male copulatory organ tube length against dorsal anchor shape. The size of dorsal anchors is proportional to the circle diameter. When anchor size and shape are similar, species that have similar size for the male copulatory organ show variation in the latter's morphology (I and II), whereas those with similar morphology of male copulatory organ show variation in the latter's size (III).

FIGURE 10. Color-coded morphological character state data for the 13 *Ligophorus* species and their estimated maximum parsimony phylogeny (1000 bootstrap replicates). a) Result using the set of morphological characters (7 to 12) that contain discretized LM1-LM3 and LM1-LM5 distances and anchor shaft shape. b) Result using anchor morphological characters derived from traditional morphometrics in Sarabeev and Desdevises (2014).

TABLE CAPTIONS

TABLE 1. GenBank accession numbers of 28S rRNA, 18S rRNA and ITS1 sequences of the 13 *Ligophorus* species, with information about the latters' host species and collection location. Sequences obtained in present study are marked with an asterisk.

TABLE 2. List of morphological characters used to construct maximum parsimony trees. All characters in Set A were taken from Sarabeev and Desdevises (2014). Characters 1-6 of Set B

are the same as Set A's; Characters 7-12 of Set B were constructed in the present study based on results of geometric morphometric analysis.

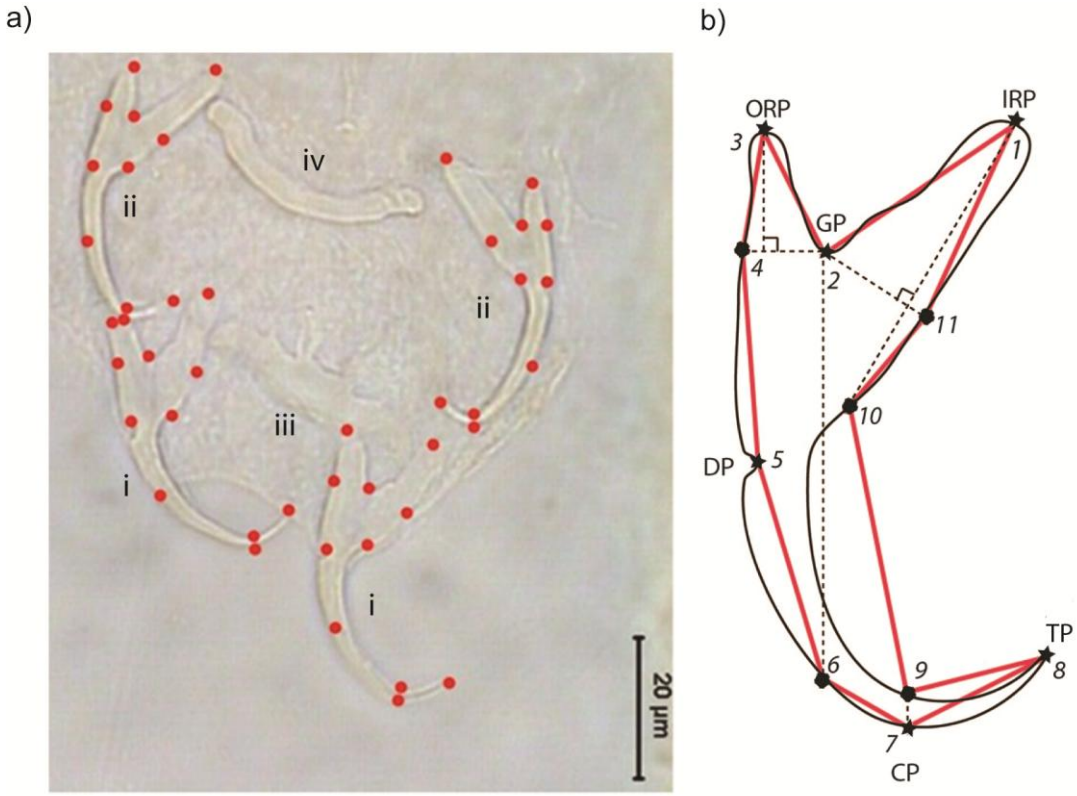

FIGURE 1. a) Landmarks of the i) ventral and ii) dorsal anchors of a *L. navjotsodhii* sample, digitized using TPSDIG2 (Version 2.17). The iii) ventral and iv) dorsal bars can also be seen in the image. b) Landmark positions on an anchor. Type I landmarks (LM1,LM2,LM3,LM5,LM7,LM8) are indicated by stars, while Type III landmarks (LM4,LM6,LM9,LM10,LM11) are indicated by solid circles. Abbreviations: ORP - outer root point; GP - groove point; IRP - inner root point; DP - dent point; CP - curve point; TP - tip point.

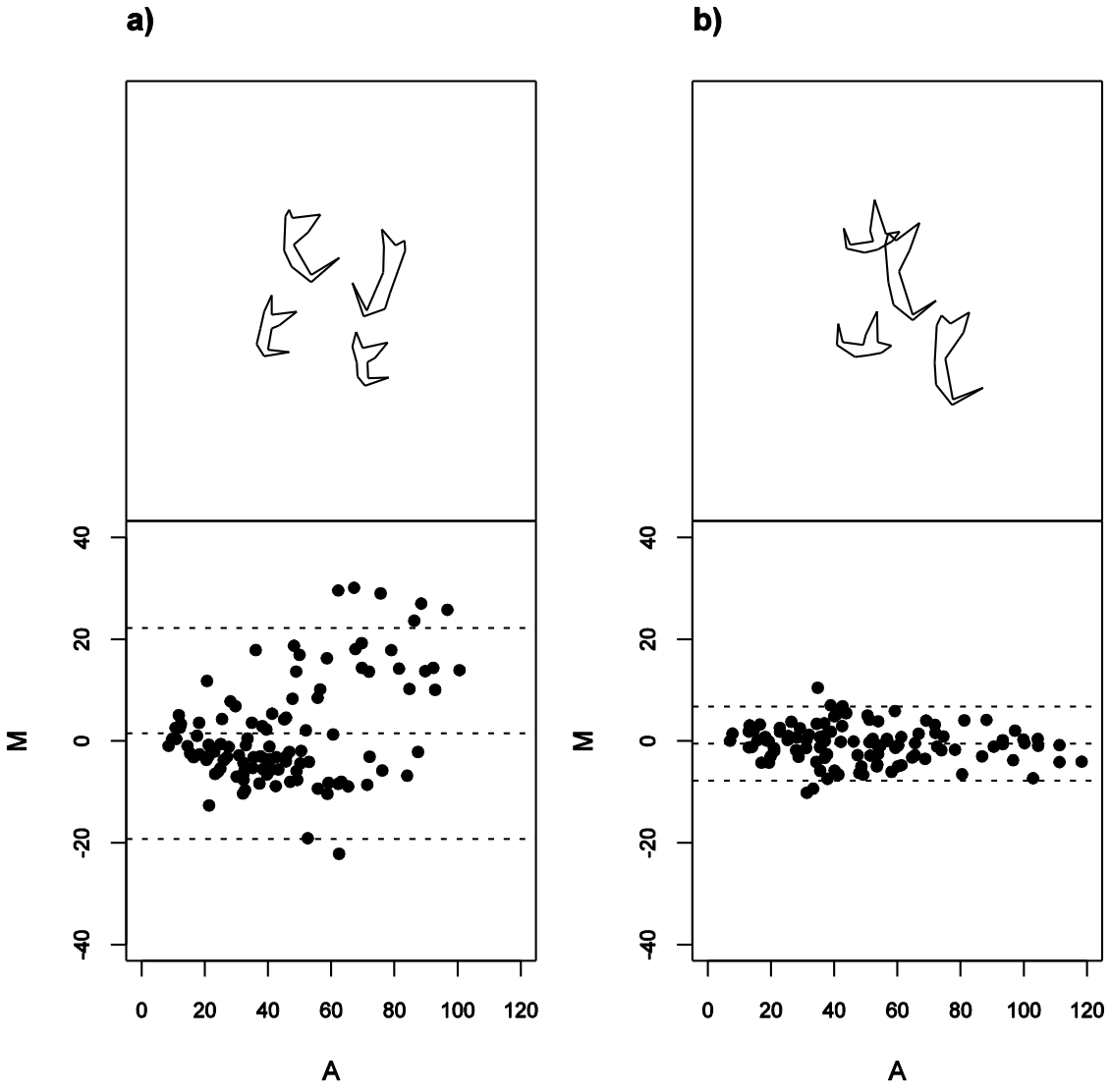

FIGURE 2. Wireframe plots of anchors of *L. bantingensis* lying in their natural positions in the mounted slide. a) Example of a poor quality specimen (Q = 1); note substantial variation between shape of (larger) left and right forms of the dorsal anchors, which shows up in a Tukey Mean Difference (TMD) plot that has relatively wide width of 95% limits of agreement (upper and lower dashed lines) as well as a fanning pattern as *A* becomes larger. b) Example of a good quality specimen (Q=40); note lack of shape variation between left and right forms of ventral and dorsal anchors, which shows up in a TMD plot with much narrower width of 95% limits of agreement as well as a more or less random deviation of *M* about 0 independent of *A*.

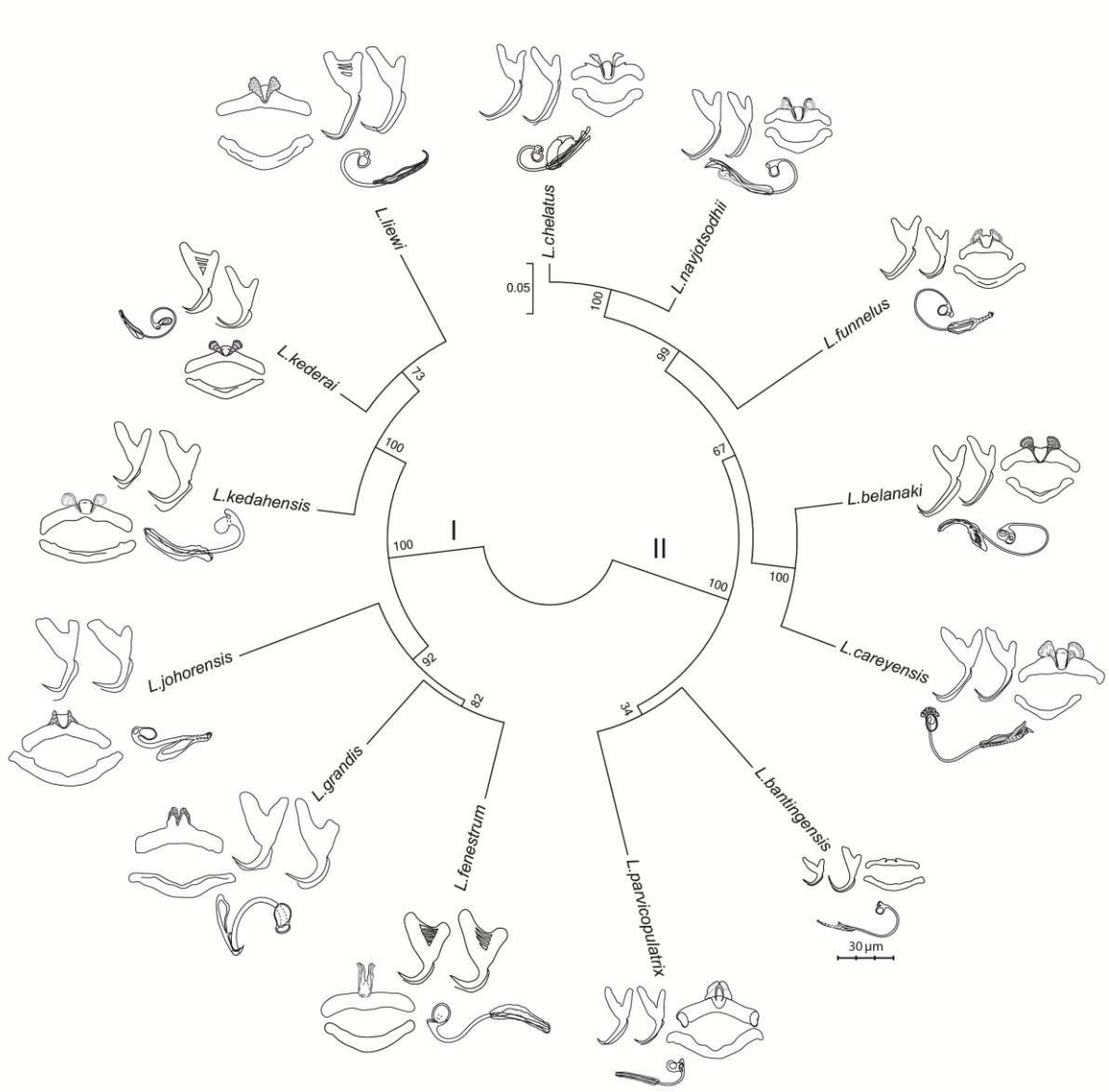

19

20 FIGURE 3. Molecular phylogeny of the 13 *Ligophorus* species inferred using the maximum
21 likelihood method (500 bootstrap replicates) with annotations from three anatomical
22 structures: anchors, bars and male copulatory organ (30% of original scale). Species in Clade
23 I are found in *Moolgarda buchanani*, and species in Clade II are found in *Liza subviridis*. The
24 ventral and dorsal forms of the anchors are arranged from left to right, those of the bars from
25 top to bottom.

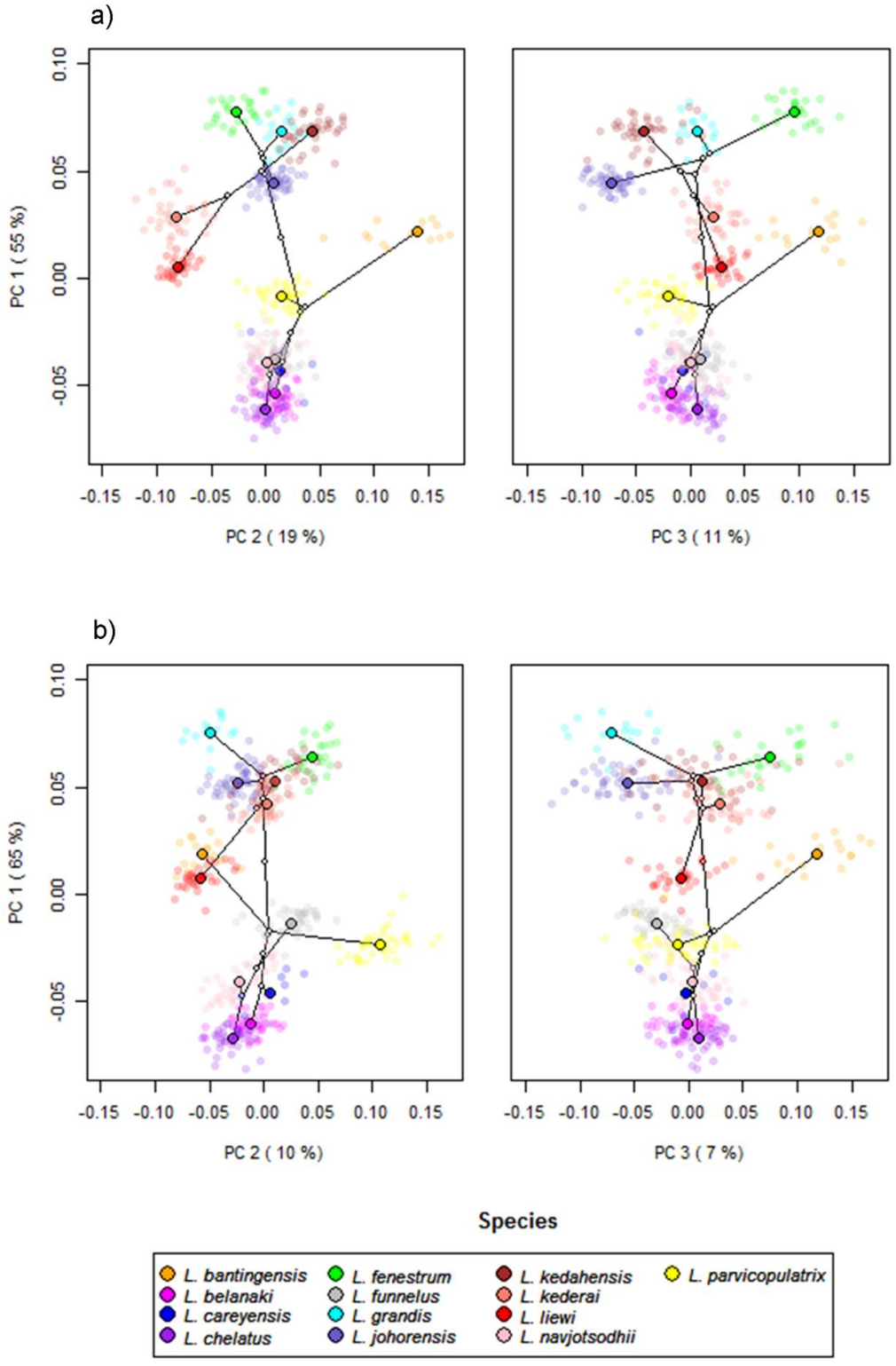

FIGURE 4. PCA plots of PC1 against PC2 and PC3 for a) ventral and b) dorsal anchors, with superimposed phylogeny of the 13 *Ligophorus* species. The centroids of the species are indicated in solid colors, while individual samples are plotted in high transparency colors.

The estimated principal component coordinates of the ancestral nodes are represented by small open circles.

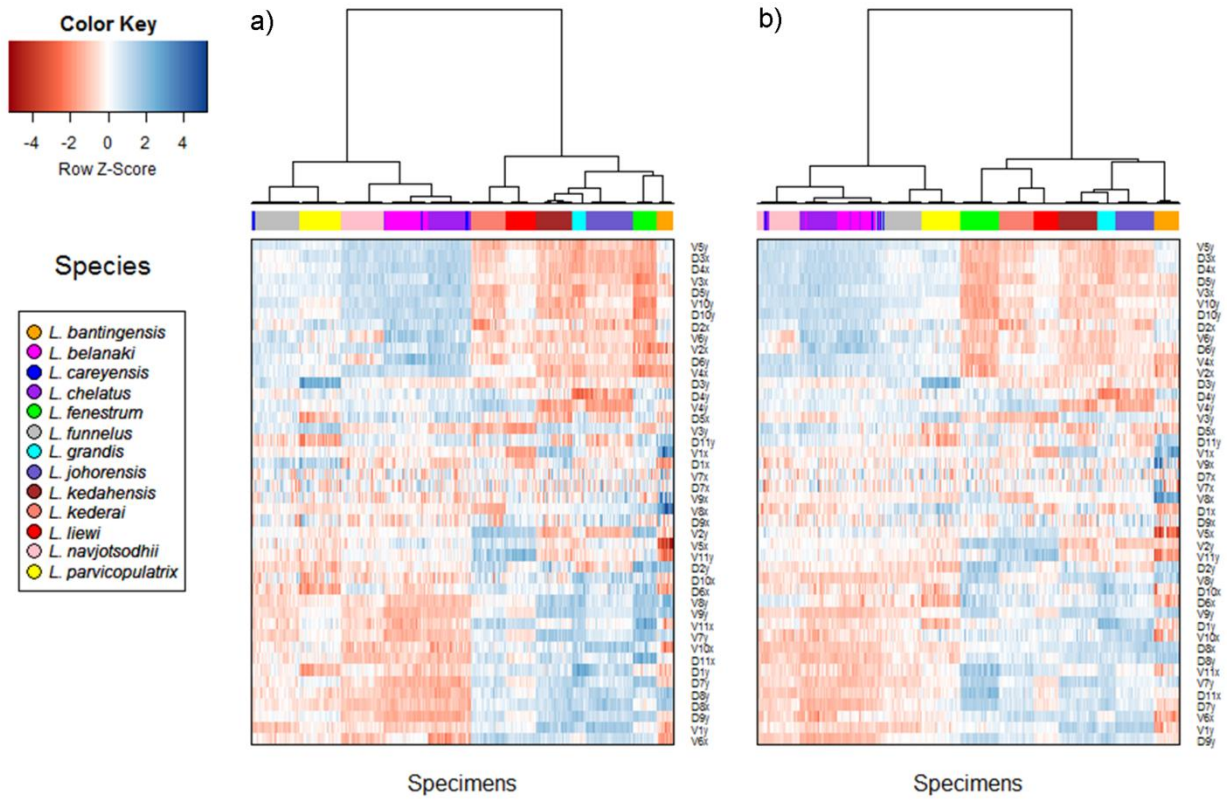

FIGURE 5. Cluster heat map of specimens (column) using shape variable data (row). The name of a shape variables consists of three parts: a prefix indicating ventral (V) or dorsal (D) anchors, a number indicating landmark index, and a suffix indicating x or y coordinate value. a) Cluster heat map using filtered specimens with quality score of 10 or more (n=443); b) Cluster heat map using all specimens (n=537).

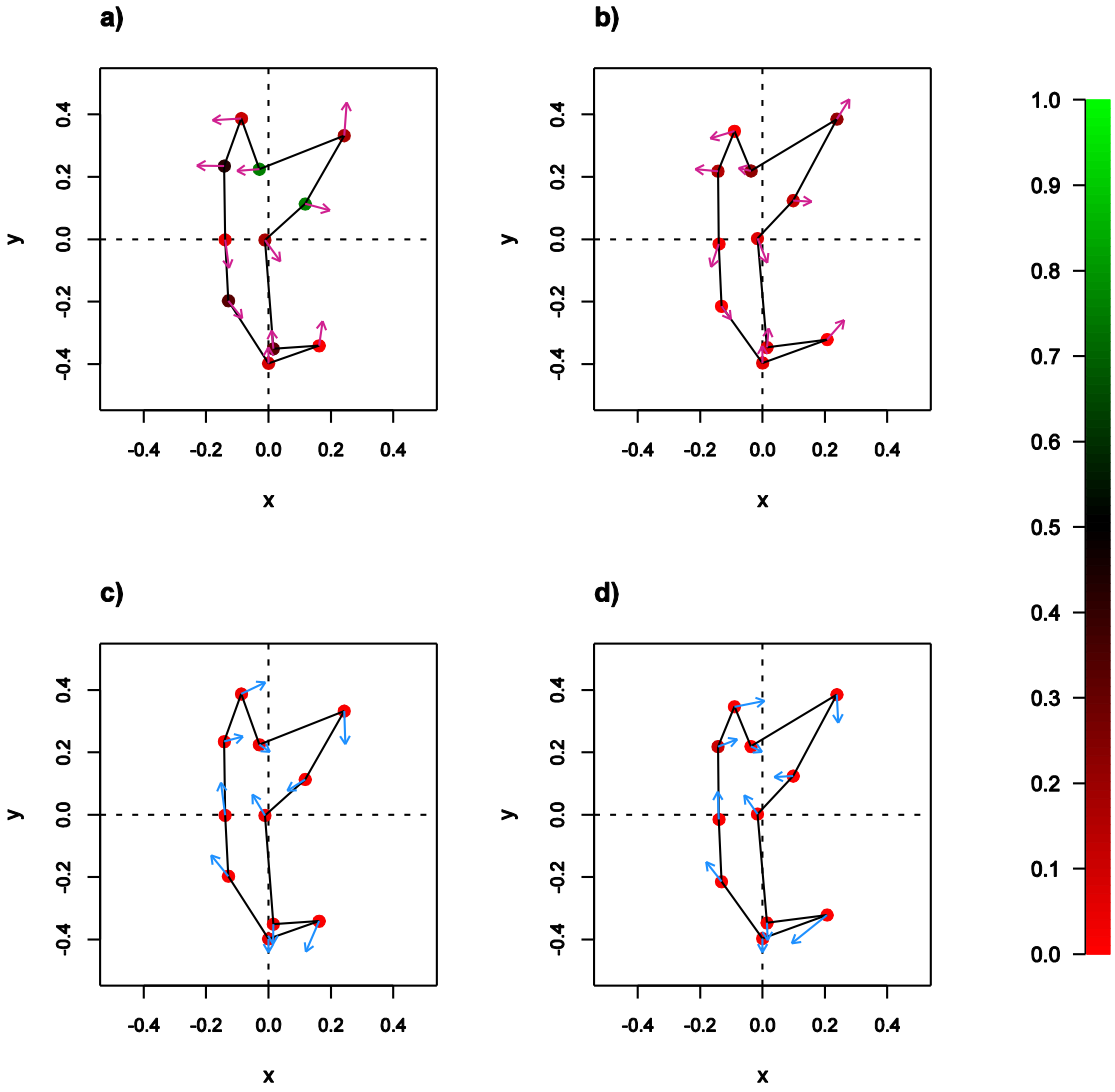

42

43 FIGURE 6. Wireframe-lollipop plots of mean shape change relative to estimated ancestral
44 mean shape in a) ventral anchors of Clade I (purple); b) dorsal anchors of Clade I; c) ventral
45 anchors of Clade II (blue); d) dorsal anchors of Clade II. The p-value of Rayleigh test for
46 uniform direction change at each landmark is indicated as a colored solid circle. The color bar
47 maps color tones to their corresponding p-values.

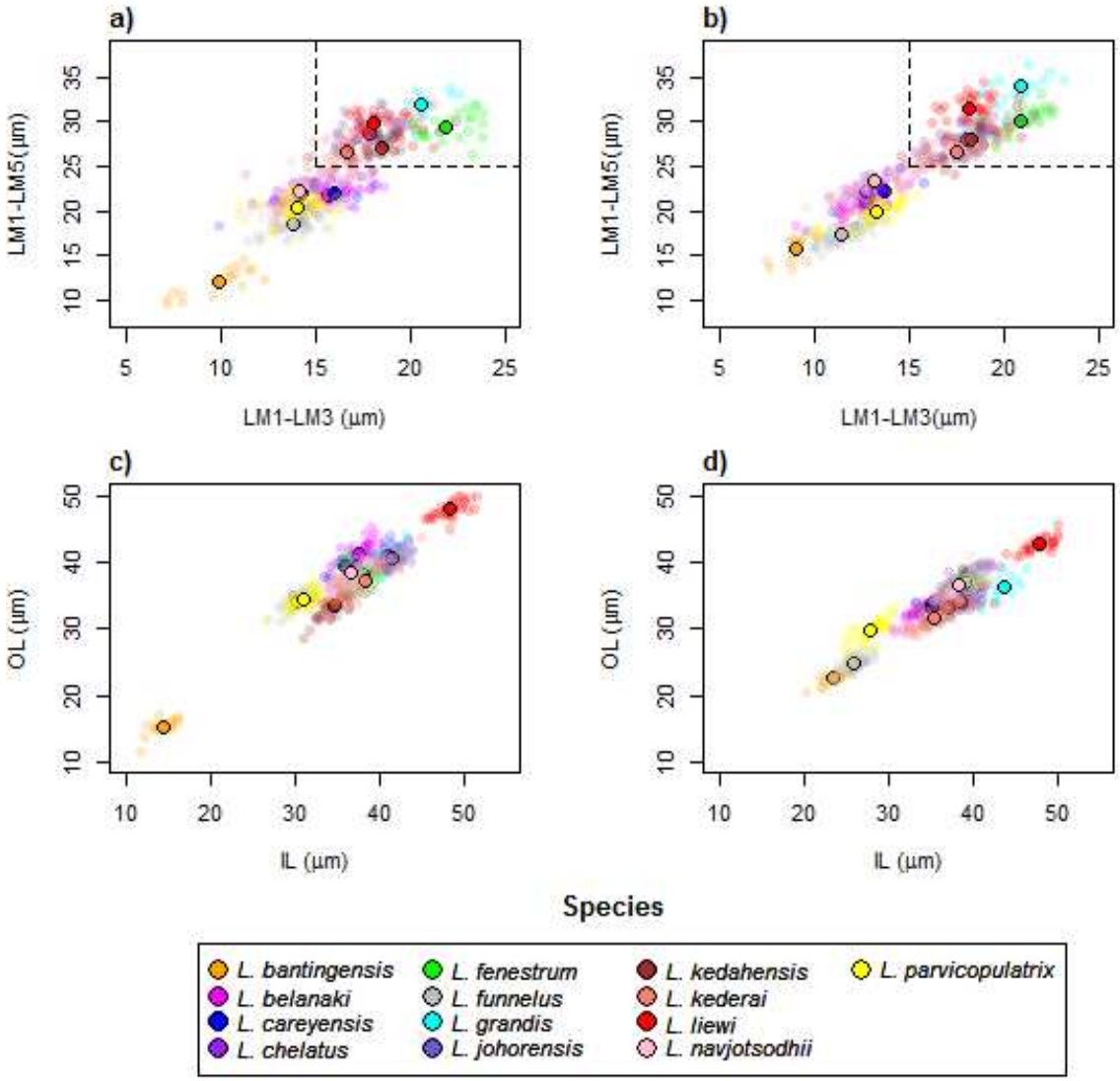

48

49 FIGURE 7. Scatter plots LM1-LM5 distance against LM1-LM3 distance for a) ventral and b)
50 dorsal anchors. The dashed lineas are cut-offs on the x and y axes that allow complete
51 discrimination of Clade I from Clade II. Scatter plots of outer length (OL) against inner
52 length (IL) for c) ventral and d) dorsal anchors. No cut-offs on the x and y axes permit
53 complete discrimination of Clade I from Clade II.

54

55

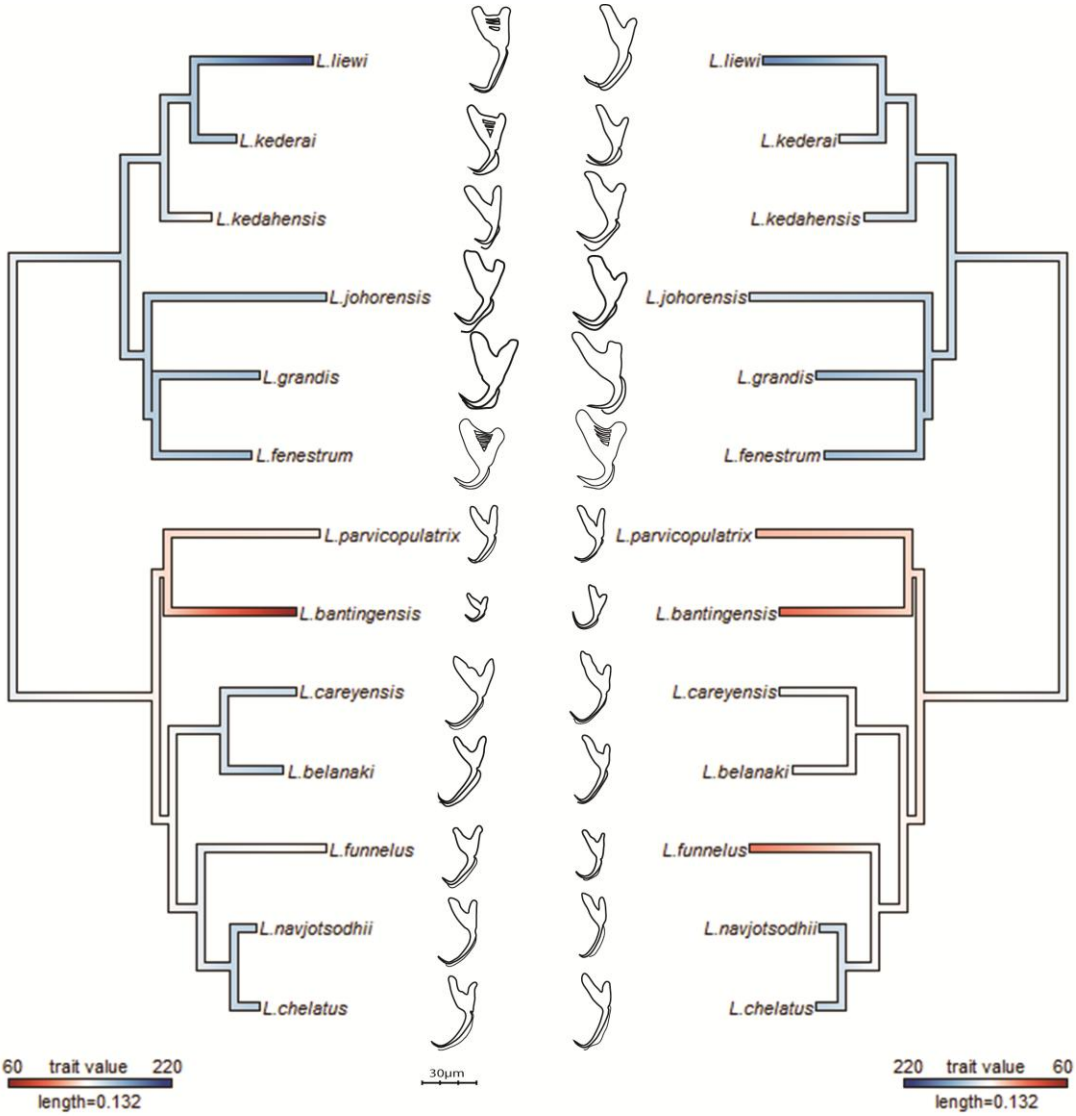

FIGURE 8. Continuous character mapping of anchor size (in µm) of ventral (left) and dorsal (right) anchor onto the maximum likelihood phylogeny of the 13 *Ligophorus* species.

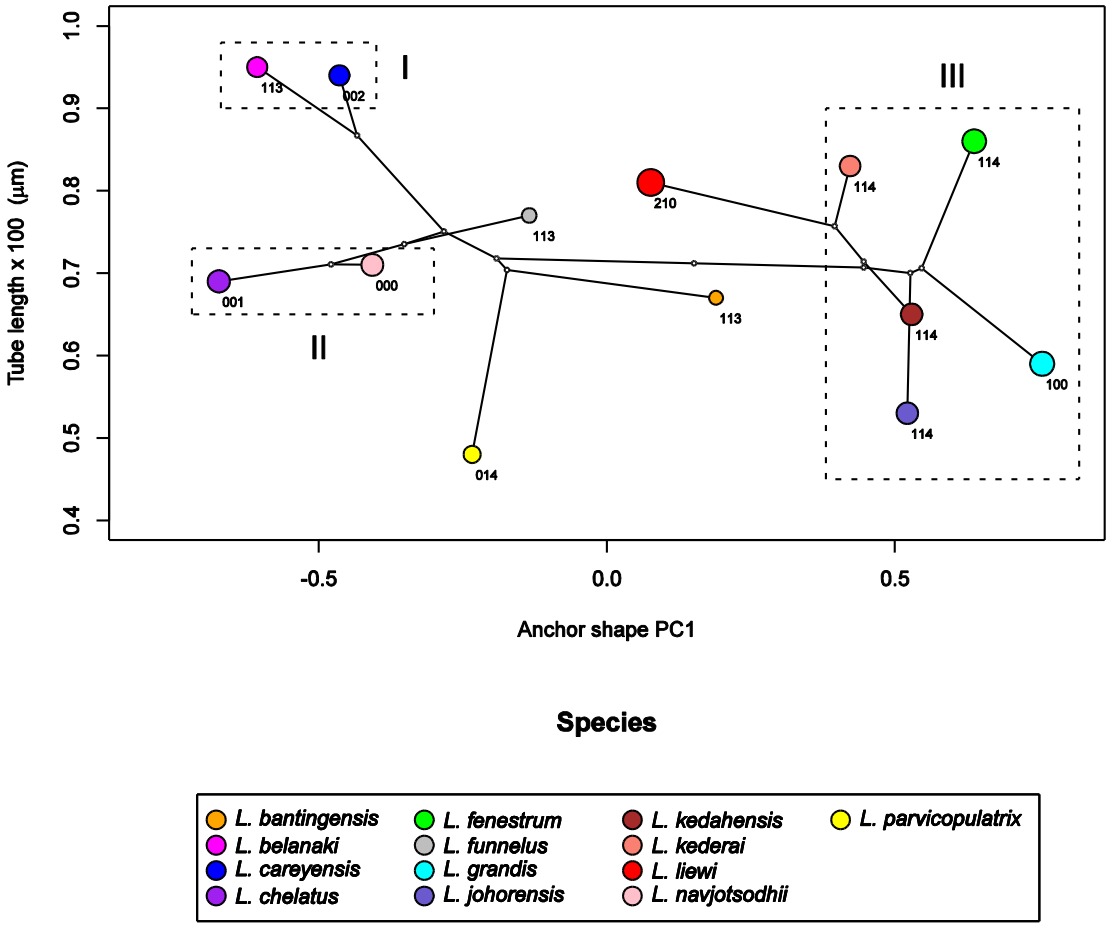

64

65 FIGURE 9. Scatter plot of male copulatory organ tube length against dorsal anchor shape.
66 The size of dorsal anchors is proportional to the circle diameter. When anchor size and shape
67 are similar, species that have similar size for the male copulatory organ show variation in the
68 latter's morphology (I and II), whereas those with similar morphology of male copulatory
69 organ show variation in the latter's size (III).

70

71

72

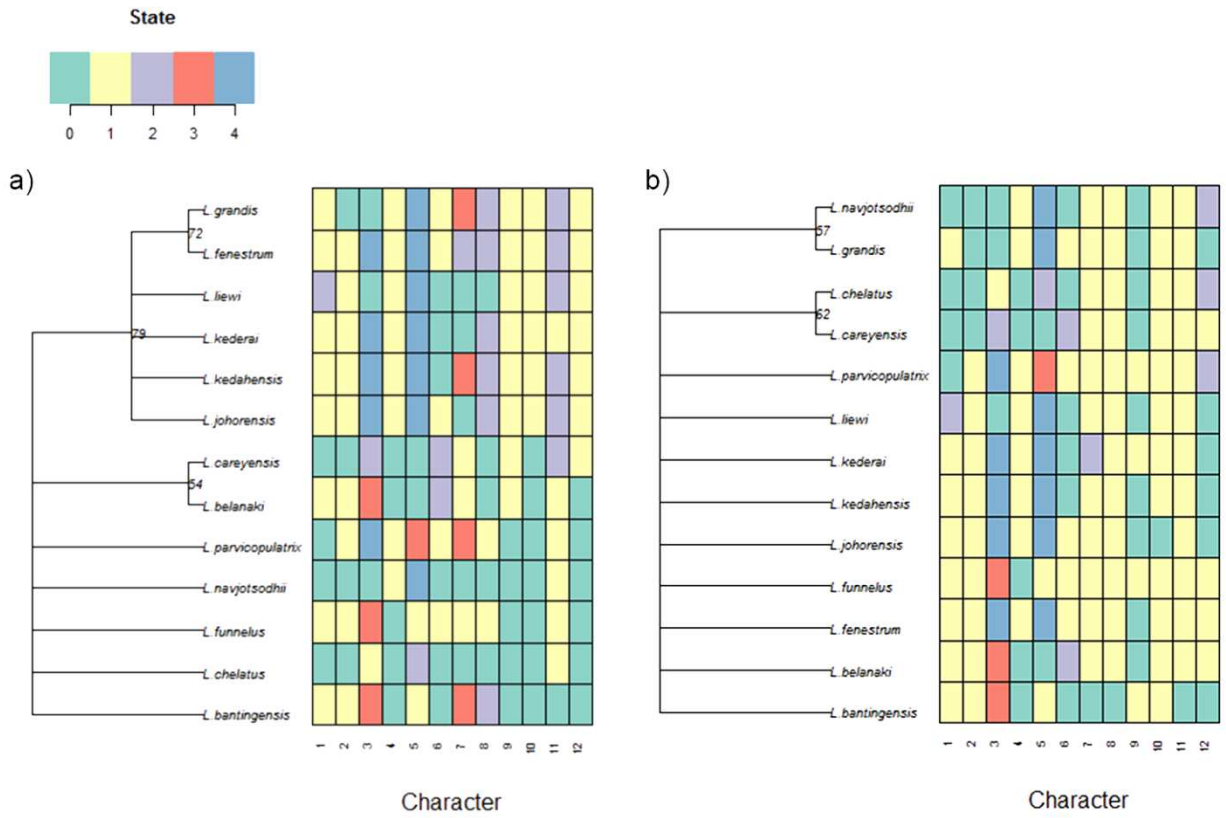

FIGURE 10. Color-coded morphological character state data for the 13 *Ligophorus* species and their estimated maximum parsimony (MP) phylogeny (1000 bootstrap replicates). a) Result using the set of morphological characters (6 to 12) that contain discretized LM1-LM3 and LM1-LM5 distances and anchor shaft shape. b) Result using anchor morphological characters derived from traditional morphometrics in Sarabeev and Desdevises (2014).

Ligophorus species	Host species	Locality (Malaysia)	GenBank Accession no.		
			28S rRNA	18S rRNA	ITS1
L. bantingensis	*Liza subviridis*	Carey Island, Selangor	KM221909	KM221934*	KM221922
L. belanaki			KM221910	KM221935*	KM221923
L. careyensis			KM221911	KM221936*	KM221924
L. chelatus			KM221912	KM221937*	KM221925
L. funnelus			KM221914	KM262663*	KM262662
L. navjotsodhii			KM221920	KM221944*	KM221932
L. parvicopulatrix			KM221921	KM221945*	KM221933
L. fenestrum	*Moolgarda buchanani*	Langkawi Island, Kedah	KM221913	KM221938*	KM221926
L. kedahensis			KM221917	KM221941*	KM221929
L. kederai			KM221918	KM221942*	KM221930
L. grandis		Straits of Johor	KM221915	KM221939*	KM221927
L. johorensis			KM221916	KM221940*	KM221928
L. liewi			KM221919	KM221943*	KM221931

TABLE 1. GenBank accession numbers of 28S rRNA, 18S rRNA and ITS1 sequences of the 13 *Ligophorus* species, with information about their host species and collection location. Sequences obtained in present study are marked with an asterisk.

PeerJ PrePrints | https://dx.doi.org/10.7287/peerj.preprints.1283v1 | CC-BY 4.0 Open Access | rec: 4 Aug 2015, publ: 4 Aug 2015

Characters	Character States	Set A		Set B	
		Included in study	Index	Included in study	Index
Male copulatory organ:					
Position of copulatory organ entrance at main lobe of accessory piece	(0) proximal; (1) distal; (2) medial	√	1	√	1
Accessory piece of male copulatory complex	(0) consists of two lobes (main and secondary lobes or proximal and distal ones); (1) consists of one lobe	√	2	√	2
Shape of accessory piece of male copulatory complex	(0) beak or hook-shaped; (1) claw-shaped pincer-like; (2) cross-shaped; (3) funnel-shaped; (4) open, grooved tube (rod-like)	√	3	√	3
Female reproductive system					
Vaginal canal sclerotization	(0) present; (1) absent	√	4	√	4
Distal end of sclerotized vagina	(0) funnel-shaped thin-walled; (1) funnel-shaped thick-walled; (2) scyphoid narrow; (3) scyphoid broad; (4) not observed	√	5	√	5
Bars					
Relative size of ventral and dorsal bar	(0) subequal; (1) dorsal bar longer than ventral one; (2) ventral bar longer than dorsal one; (3) not applicable	√	6	√	6
Anchors					
Ratio of shaft to point of ventral anchor	(0) less than 1.4; (1) 1.4–2.6; (2) greater than 2.6	X	-	√	7
Ratio of shaft to point of dorsal anchor	(0) less than 1.4; (1) 1.4–2.6; (2) greater than 2.6	X	-	√	8
Length of ventral anchor point	(0) 7–12 µm; (1) less than 7 µm	X	-	√	9

PeerJ PrePrints | https://dx.doi.org/10.7287/peerj.preprints.1283v1 | CC-BY 4.0 Open Access | rec: 4 Aug 2015, publ: 4 Aug 2015

Characters	Character States	Set A		Set B	
		Included in study	Index	Included in study	Index
Length of dorsal anchor point	(0) greater than 11 µm; (1) 5–11 µm; (2) less than 5 µm	X	-	√	10
Relation of outer root to point of ventral anchor	(0) outer root shorter than point; (1) outer root subequal or longer than point	X	-	√	11
Relation of outer root to point of dorsal anchor	(0) outer root shorter than point; (1) outer root subequal with point; (2) outer root longer than point	X	-	√	12
New characters					
Shape of ventral anchor	(0) shaft scimitar-shaped, root U-shaped (1) shaft scimitar-shaped, root V-shaped; (2) shaft sickle-shaped, root U-shaped; (3) shaft sickle-shaped, root V-shaped	√	7	X	-
Shape of dorsal anchor	(0) shaft scimitar-shaped, asymmetric inner and outer roots; (1) shaft sickle-shaped, symmetric inner and outer roots; (2) shaft sickle-shaped, asymmetric inner and outer roots	√	8	X	-
Ventral anchor: Length from L1 to L3	(0) 15µm or less; (1) greater than 15µm	√	9	X	-
Dorsal anchor: Length from L1 to L3	(0) 15µm or less; (1) greater than 15µm	√	10	X	-
Ventral anchor: Length from L1 to L5	(0) Less than 15µm; (1) 15µm - 25µm; (2) greater than 25µm	√	11	X	-
Dorsal anchor: Length from L1 to L5	(0) 15µm - 25µm; (1) greater than 25µm	√	12	X	-

PeerJ PrePrints | https://dx.doi.org/10.7287/peerj.preprints.1283v1 | CC-BY 4.0 Open Access | rec: 4 Aug 2015, publ: 4 Aug 2015

TABLE 2. List of morphological characters used to construct maximum parsimony trees. All characters in Set A were taken from Sarabeev and Desdevises (2014). Characters 1-6 of Set B are the same as Set A's; Characters 7-12 of Set B were constructed in the present study based on results of geometric morphometric analysis.

PeerJ PrePrints | https://dx.doi.org/10.7287/peerj.preprints.1283v1 | CC-BY 4.0 Open Access | rec: 4 Aug 2015, publ: 4 Aug 2015